AGU PUBLICATIONS

Journal of Advances in Modeling Earth Systems

RESEARCH ARTICLE
10.1002/2017MS001248

**Key Points:**
- Warm-season rainfall increased observed latent heat flux that the Community Land Model (CLM) did not replicate without adjustments to the model parameterization
- Examples of sensitivity tests to land-surface model parameterizations and parameters are shown
- Drainage flows in complex terrain increased near-ground turbulence and enhanced nocturnal evaporation, which is a process typically not within land-surface models

**Supporting Information:**
- Supporting Information S1
- Data Set S1

**Correspondence to:**
S. P. Burns,
sean@ucar.edu

**Citation:**
Burns, S. P., Swenson, S. C., Wieder, W. R., Lawrence, D. M., Bonan, G. B., Knowles, J. F., & Blanken, P. D. (2018). A comparison of the diel cycle of modeled and measured latent heat flux during the warm season in a Colorado subalpine forest. *Journal of Advances in Modeling Earth Systems*, *10*, 617–651. https://doi.org/10.1002/2017MS001248

Received 22 NOV 2017
Accepted 25 JAN 2018
Accepted article online 2 FEB 2018
Published online 8 MAR 2018



# A Comparison of the Diel Cycle of Modeled and Measured Latent Heat Flux During the Warm Season in a Colorado Subalpine Forest

**Sean P. Burns[1,2], Sean C. Swenson[2], William R. Wieder[2,3], David M. Lawrence[2], Gordon B. Bonan[2], John F. Knowles[3,4], and Peter D. Blanken[1]**

[1]Department of Geography, University of Colorado, Boulder, CO, USA, [2]National Center for Atmospheric Research, Boulder, CO, USA, [3]Institute of Arctic and Alpine Research, University of Colorado, Boulder, CO, USA, [4]School of Geography and Development, University of Arizona, the College of Social and Behavioral Sciences, Tucson, AZ, USA

**Abstract** Precipitation changes the physiological characteristics of an ecosystem. Because land-surface models are often used to project changes in the hydrological cycle, modeling the effect of precipitation on the latent heat flux $\lambda E$ is an important aspect of land-surface models. Here we contrast conditionally sampled diel composites of the eddy-covariance fluxes from the Niwot Ridge Subalpine Forest AmeriFlux tower with the Community Land Model (CLM, version 4.5). With respect to measured $\lambda E$ during the warm season: for the day following above-average precipitation, $\lambda E$ was enhanced at midday by ≈40 W m$^{-2}$ (relative to dry conditions), and nocturnal $\lambda E$ increased from ≈10 W m$^{-2}$ in dry conditions to over 20 W m$^{-2}$ in wet conditions. With default settings, CLM4.5 did not successfully model these changes. By increasing the amount of time that rainwater was retained by the canopy/needles, CLM was able to match the observed midday increase in $\lambda E$ on a dry day following a wet day. Stable nighttime conditions were problematic for CLM4.5. Nocturnal CLM $\lambda E$ had only a small (≈3 W m$^{-2}$) increase during wet conditions, CLM nocturnal friction velocity $u_*$ was smaller than observed $u_*$, and CLM canopy air temperature was 2°C less than those measured at the site. Using observed $u_*$ as input to CLM increased $\lambda E$; however, this caused CLM $\lambda E$ to be increased during both wet and dry periods. We suggest that sloped topography and the ever-present drainage flow enhanced nocturnal $u_*$ and $\lambda E$. Such phenomena would not be properly captured by topographically blind land-surface models, such as CLM.

## 1. Introduction

Precipitation is a common perturbation that changes the physical and physiological properties of a forest ecosystem. The most immediate effect is the wetting of vegetation and ground surfaces to provide liquid water for evaporation which changes the surface energy partitioning between sensible heat flux $H$ and latent heat flux $\lambda E$. There is a long history of research into how canopy interception of precipitation modifies the water and energy budgets of an ecosystem (e.g., Kang et al., 2012; Klaassen, 2001; Kume et al., 2008; Moors, 2012; Rutter et al., 1975; Shuttleworth, 2007; Stewart, 1977; van Dijk et al., 2015). Such changes are important in the modeling of ecosystem process on both local and global scales (e.g., Bonan, 2008; Bosveld & Bouten, 2003).

Our study uses data from a high-elevation subalpine forest AmeriFlux site (US-NR1) to explore how warm-season rain events (defined as a daily precipitation total greater than 3 mm) affects the above-canopy turbulent energy fluxes of latent and sensible heat. The warm season is defined as the period between complete snowpack ablation and diminished forest photosynthesis (roughly, early June to early October). During this period, almost all precipitation is rain, not snow. Burns et al. (2015) has shown that warm-season precipitation caused changes to the midday latent and sensible heat fluxes on the order of 50–70% at the same subalpine forest that is the focus of the current study. Herein, we extend that work to compare the measured above-canopy sensible and latent heat fluxes to those from a land-surface model, where the model is driven using meteorological and radiation data measured from a tower above the forest. From an analysis of the diel cycle, we evaluate both the magnitude and timing of how the measured and modeled energy fluxes are modified by the presence of rainwater in the soil and on the vegetation (we use the term "diel" to emphasize that we are looking at the full 24 h cycle, not only daytime [diurnal] and nighttime

[nocturnal] periods). In this study, we focus on two specific aspects of $\lambda E$ related to warm-season rainfall at US-NR1: (i) for a dry day following a day with above-average precipitation, midday $\lambda E$ reached a peak value near 220 W $m^{-2}$ (compared to 180 W $m^{-2}$ for a dry day preceded by a dry day) and (ii) nocturnal $\lambda E$ increased from ≈10 W $m^{-2}$ in dry conditions to over 20 W $m^{-2}$ in wet conditions (Burns et al., 2015).

To study the model physics, it is advantageous to examine the full diel cycle (e.g., Matheny et al., 2014). From the diel cycle, the timing of modeled phenomena, such as canopy evaporation, can be examined. The other advantage of analyzing the full diel cycle is that most land-surface exchange processes are very different at night compared to the daytime, primarily due to the effects of solar radiation on energy transformations. Radiative effects also change the atmospheric physics, such as the atmospheric stability. Historically, strongly stable conditions have been especially difficult to model due to the breakdown of the validity of Monin-Obukhov Similarity Theory (MOST) and issues such as surface-atmosphere decoupling and runaway cooling of the ground surface (e.g., Aubinet, 2008; Holtslag et al., 2013; Mahrt, 1999). Runaway cooling occurs in models due to a positive feedback between the surface temperature and turbulence, where a cold surface temperature limits the turbulent exchange at the surface, which leads to an even colder surface temperature, and so on. Typically, MOST provides the theoretical underpinnings used by land-surface models. The key points about MOST relevant to our study are described in section 3.7.1.

Land-surface models typically view vegetation as either a single layer "big leaf" or resolve multiple vertical levels within the vegetation using a so-called multilayer modeling approach. Not surprisingly, there are trade-offs in complexity/simplicity and computational speed with each approach. For both approaches, the primary challenge is the determination of resistance parameters to the transfer of momentum and scalars between the surface and atmosphere (e.g., Raupach & Finnigan, 1988).

The model we use for our study is the Community Land Model (CLM; Oleson et al., 2013). CLM uses a big-leaf approach to model the effect of vegetation on the land-surface exchange; however, individual processes are uniquely calculated within the model. For example, latent heat flux has uniquely parameterized schemes for soil evaporation (Swenson & Lawrence, 2014), canopy evaporation (Lawrence et al., 2007; Oleson et al., 2008), and transpiration (Bonan et al., 2014). The sum of these individual component terms (transpiration, ground evaporation, and canopy evaporation) produces the CLM latent heat flux. Several of the equations and constants within the CLM subcanopy turbulence parameterizations can be traced back to the Biosphere-Atmosphere Transfer Scheme (BATS; Dickinson et al., 1993) which was formulated over 25 years ago. Though certain components of CLM have been updated and investigated quite rigorously, there have only been a few studies related to the subcanopy turbulence (e.g., Sakaguchi & Zeng, 2009; Zeng et al., 2005) and a thorough sensitivity analysis is overdue.

Because these parameterizations affect the latent heat flux, they are relevant to our study and we perform a sensitivity analysis on several aspects of CLM, with an emphasis on the turbulence parameterization (details in sections 3.7 and 3.8). The aspects of CLM that we examine are (1) sensitivity to leaf area index (LAI), which we expect to be an important factor controlling the CLM fluxes (e.g., Lawrence et al., 2007), (2) varying the CLM internal variable *maximum leaf wetted fraction* $f_{wet}^{max}$ which controls how long precipitation resides on the vegetation surfaces, (3) replacing CLM-modeled friction velocity $u_*$ with that measured on the tower, (4) using different forms of the so-called universal functions for modeling the vertical exchange of momentum, sensible, and latent heat (e.g., Foken, 2006, 2008), and (5) varying two internal CLM variables: the subcanopy turbulent exchange coefficient, $C_{s,dense}$, and *zetamaxstable* $\zeta_{stable}^{max}$ which sets an upper limit on the stable side of the universal functions.

Another primary objective of our study is to provide a framework for evaluating models and observations at the diel-cycle scale. Systematic approaches to improving land-surface models have recently been suggested by the hydrology community (e.g., Clark et al., 2015). Though flux measurements from towers have often been used to compare, constrain, and evaluate land-surface models (e.g., Bonan et al., 2011, 2012; Lawrence et al., 2011; Pyles et al., 2000; Raczka et al., 2016; Stöckli et al., 2008; Swenson & Lawrence, 2014, among many others), in many of these studies, the focus is on large-scale/global effects of model performance over different landscapes. This is a necessary first step because land-surface models such as CLM need to run at different locations and ecosystems worldwide (from forests, to crops, to polar regions, to urban areas). Here we run CLM at a single forested site (US-NR1), using the diel cycle to examine the model performance. What is unique and different about our study is that we conditionally sample the diel cycle to focus our analysis on the effect of warm-season precipitation on the CLM fluxes and temperature. Similar techniques have been used for

analysis of observations (e.g., Betts & Ball, 1995; Burns et al., 2015; Turnipseed et al., 2009); however, such techniques have rarely (as far as we have found) been applied to the diel cycle of model output.

Because US-NR1 is in complex, mountainous terrain there are potential issues related to drainage flows and horizontal advection that need to be considered (e.g., Finnigan, 2008). As a step toward a better understanding of these issues, we have included observations from the Howland Forest AmeriFlux site (US-Ho1) in our study. US-Ho1 was chosen because it has a canopy density similar to US-NR1 but is in a location that is relatively flat compared to US-NR1. Though we do not perform a comprehensive analysis of the US-Ho1 data, we contrast the US-Ho1 and US-NR1 measurements to highlight potential effects of sloping terrain on the measurements and model performance, especially as related to the nocturnal latent heat flux.

## 2. Data and Methods

### 2.1. Site Descriptions

Our study uses data from the Niwot Ridge Subalpine Forest AmeriFlux site (site US-NR1; Blanken et al., 1998-present) located in the Rocky Mountains of Colorado. The US-NR1 measurements started in November 1998. The site is on the side of an ancient moraine with granitic-rocky-podzolic soil (typically classified as a loamy sand in dry locations) overlain by a shallow layer (≈10 cm) of organic material (Gable & Madole, 1976; Madole, 1969; Marr, 1961; Scott-Denton et al., 2003). The tree density near the US-NR1 26 m walk-up scaffolding tower is around 4,000 trees $ha^{-1}$ with a leaf area index (LAI) of 3.8–4.2 $m^2$ $m^{-2}$ and tree heights of 12–13 m (Monson et al., 2010; Turnipseed et al., 2002). The roughness length for momentum $z_{0m}$ and displacement height $d$ were determined by Turnipseed et al. (2003) to be $z_{0m} = 1.6$ m and $d = 7.8$ m. The subalpine forest surrounding the US-NR1 tower was established in the early 1900s following logging operations and is primarily composed of subalpine fir and Englemann spruce west of the tower, and lodgepole pine east of the tower. Though the tower is located in a relatively flat area (slope angle $\approx 4.3°$), the Continental Divide is 7 km to the west and 600 m higher than the site, which generates a persistent nocturnal downslope wind at the site (Burns et al., 2011). Further details about US-NR1 site have been documented elsewhere (e.g., Burns et al., 2015; Knowles et al., 2015a; Monson et al., 2002).

The Howland Forest AmeriFlux site (site US-Ho1; Hollinger, 1996-present) serves as a contrast to the US-NR1 site. The US-Ho1 site is located in a spruce-hemlock forest in Maine with a tree density of around 2,600 trees $ha^{-1}$, LAI of 5.5, and tree heights on the order of 20 m (Hollinger et al., 1999). The landscape at the site can be considered "rolling hills," with a maximum elevation change of less than 68 m within a 10 km area. The US-Ho1 site was chosen because it has a forest of comparable density to that of US-NR1, but without the nocturnal slope flow found at US-NR1 (US-Ho1 also has a long data record, measurements there started in 1996). Further details about the US-Ho1 site are in Hollinger et al. (1999, 2004).

### 2.2. The Community Land Model (CLM)

For our study, the Community Land Model (CLM) version 4.5 (CLM4.5; Oleson et al., 2013) was run in single-point mode driven with satellite phenology and 30-min US-NR1 tower observations. The above-canopy tower observations used for model input were: horizontal wind speed $U$, air temperature $T_a$, relative humidity $RH$, barometric pressure $P$, precipitation, and incoming shortwave and longwave radiation. The CLM soil texture was set to a loamy sand (72% sand, 27% silt, and 1% clay), based on a soil sample taken near the tower and analyzed by the Soil, Water and Plant Testing Laboratory at Colorado State University (N. Trahan, personal communication, 2015). In CLM, the appropriate plant functional type for US-NR1 is a temperate needleleaf evergreen forest. For this plant type, CLM assumes a canopy height $h$ of 17 m, momentum roughness length $z_{0m}$ of $0.055h$, and displacement height $d$ of $0.67h$ (Oleson et al., 2013). Modifying the CLM4.5 value for $h$ affected our our results; therefore, we chose a CLM4.5 $h$ that was closer to that of the US-NR1 forest (details are in Appendix A). For ease of comparison, we use the same nomenclature as that of Oleson et al. (2013), and the symbols and variables used in our study are in Appendix B. Specific changes made to variables or settings for different CLM4.5 configurations used in our study are listed in Table 1.

### 2.3. Analysis Methods

#### 2.3.1. Categorizing Precipitation

To study the impact of rain on the turbulent fluxes, we followed a methodology that is fully described in Burns et al. (2015). Briefly, based on 14 warm seasons (1999–2003 and 2006–2014) at US-NR1, days when

**Table 1**
*Modifications to CLM4.5 as Part of the Sensitivity Experiments*

| CLM4.5 configuration name | CLM4.5 variables and settings used for each configuration | | | | | | Notes/long description |
|---|---|---|---|---|---|---|---|
| | Form of universal function | $u_*$ source[a] | ($\zeta^{max}_{stable}$)[b] | ($f^{max}_{wet}$)[c] | S-Z[d] | ($C_{s,dense}$)[e] | |
| A1 | Zeng et al. (1998) | CLM | 2 | 1 | S-Z | 0.004 | Changed default soil texture (43% sand, 21% clay) to a value more appropriate for the US-NR1 site (72% sand, 1% clay); the CLM4.5 canopy height was also set to 13 m (see Appendix A for details) |
| B0 | Zeng et al. (1998) | CLM | 2 | 0.02 | S-Z | 0.004 | Test the impact of varying $f^{max}_{wet}$ |
| B1 | Zeng et al. (1998) | CLM | 2 | 0.02 | na | 0.004 | |
| B2 | Zeng et al. (1998) | Obs | 100 | 0.02 | na | 0.004 | |
| C0 | Zeng et al. (1998) | Obs | 2 | 1 | S-Z | 0.004 | Test the impact of using observed $u_*$ |
| D0 | Zeng et al. (1998) | CLM | 100 | 1 | S-Z | 0.004 | Test the impact of varying *zetamaxstable* $\zeta^{max}_{stable}$ |
| D1 | Zeng et al. (1998) | Obs | 100 | 1 | na | 0.004 | Test the impact of varying the universal function form |
| D2 | Högström (1988) | Obs | 100 | 1 | na | 0.004 | |
| D3 | Handorf et al. (1999) | Obs | 100 | 1 | na | 0.004 | |
| E0 | Zeng et al. (1998) | CLM | 2 | 1 | na | 0.004 | Test the impact of turning off S-Z (Sakaguchi & Zeng, 2009) |
| F0 | Zeng et al. (1998) | CLM | 2 | 1 | S-Z | 0.01 | Test the impact of varying $C_{s,dense}$ |
| F1 | Zeng et al. (1998) | CLM | 2 | 1 | na | 0.01 | |
| F2 | Zeng et al. (1998) | Obs | 100 | 1 | na | 0.01 | |
| G1 | Högström (1988) | Obs | 100 | 0.02 | na | 0.01 | Changes made to all variables |

*Note*. The alphanumeric codes in the first column are used throughout the text and figures to specify the configuration used for CLM4.5. The default configuration is "CLM4.5 A1," and a numerical value of "0" indicates a single variable has been modified from the CLM4.5 A1 configuration.

[a]"Obs" indicates that US-NR1 observed friction velocity $u_*$ was used as input to CLM; "CLM" indicates CLM4.5-calculated $u_*$ was used. [b]The value of *zetamaxstable* $\zeta^{max}_{stable}$ (CLM4.5 default: $\zeta^{max}_{stable}=2$). [c]The value of *maximum leaf wetted fraction* $f^{max}_{wet}$ (CLM4.5 default: $f^{max}_{wet}=1$). [d]"S-Z" indicates that the subcanopy stability correction proposed by Sakaguchi and Zeng (2009) was used; "na" indicates it was not used. [e]The value of the subcanopy turbulent transfer coefficient $C_{s,dense}$ (CLM4.5 default: $C_{s,dense}=0.004$).

the daily rainfall exceeded 3 mm were tagged as "wet" days. We then classified the warm-season days as "dry days following a dry day" (dDry days), "wet days following a dry day" (dWet days), "wet days following a wet day" (wWet days), and "dry days following a wet day" (wDry days) where the lower case letter designates the precipitation state of the preceding day. An example of classifying the data in this way is shown in Figure 1. The summers of 2004 and 2005 were excluded from our analysis because downwelling longwave radiation was not available to use as input to CLM. The number of 30-min samples that were in each precipitation category are listed at the bottom of Table 2 and in Figure 1a. In our discussion, the term "wet days" includes both dWet and wWet days whereas the term "dry days" includes both dDry and wDry days. In addition to these categories, dDry days with clear skies were designated as dDry-Clear days. For the analysis, days with a similar precipitation state were lumped together and composite diel cycles were created. In the composite diel cycle, we calculated both the mean and standard deviation. The standard deviation represents the amount of day-to-day variability within the diel cycle which we designate as the SD-Bin or variability in our plots and discussion. Within our analysis, the CLM4.5 and measured variables were treated exactly the same—so results come from time periods when the measurements and CLM output both existed.

### 2.3.2. Categorizing Atmospheric Stability

When examining atmospheric stability near the ground a useful variable is the bulk Richardson number $Ri_b$. Large negative $Ri_b$ indicates unstable "free convection" conditions and large positive $Ri_b$ indicates strong stability. In more stable conditions, less mixing is expected and larger vertical scalar gradients should exist. We calculated $Ri_b$ between the highest ($z_2=21.5$ m, around twice canopy height) and lowest ($z_1=2$ m) measurement level using

$$Ri_b = \frac{g}{\bar{T}_a}\frac{(\theta_2-\theta_1)(z_2-z_1)}{U^2}, \quad (1)$$

where $g$ is acceleration due to gravity, $\bar{T}_a$ is the average air temperature of the layer, $\theta$ is potential temperature, and $U$ is the above-canopy horizontal vectorial mean wind speed (i.e., $U=(u^2+v^2)^{1/2}$ where $u$ and $v$

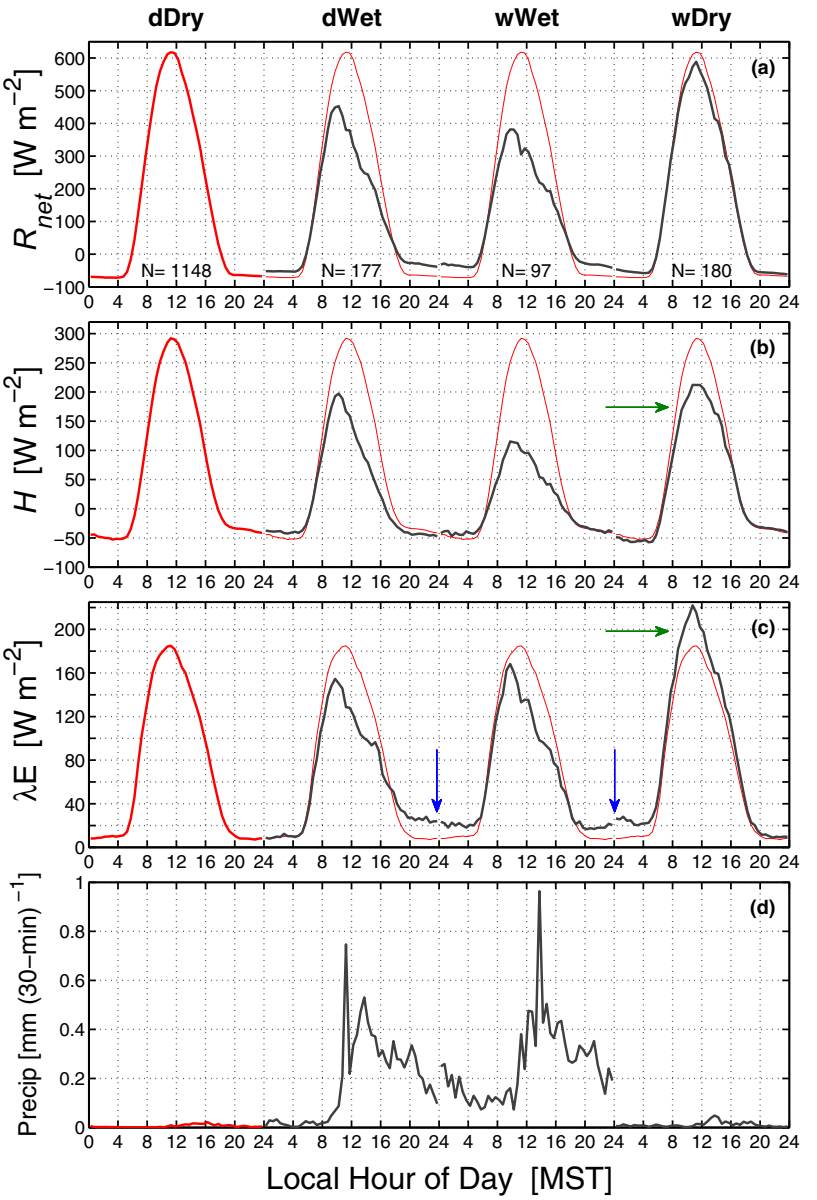


**Figure 1.** The mean warm-season composite diel cycle of (a) net radiation $R_{net}$, (b) sensible heat flux $H$, (c) latent heat flux $\lambda E$, and (d) precipitation for each precipitation state (dDry, dWet, wWet, and wDry) where the precipitation state for each diel cycle is identified above Figure 1a. For reference, the dDry diel cycle is repeated for all states as a red line. In Figures 1b and 1c, the arrows refer to discussion points within the text. The diel cycle is calculated from 30 min measurements during the warm season for years 1999–2003 and 2006–2014 with the approximate number of days ($N$) used to create each composite shown in Figure 1a. More information on the measurements, precipitation state, and data compositing are within the text.

are the streamwise and crosswise planar-fit horizontal wind components). In CLM4.5, $Ri_b$ is used to determine an initial guess at $\zeta$ and $L$ which are then used to iteratively determine the vertical gradients of wind and scalars (Oleson et al., 2013).

As shown by Burns et al. (2011), in strongly stable conditions $Ri_b$ provides an extra 2 logarithmic decades where $\zeta$ is nearly constant. For this reason, we will use $Ri_b$ to examine the variables and parameters in strongly stable conditions.

### 2.3.3. Statistical Evaluation of Results

As will be shown more explicitly in section 3, the focus in this paper is on two specific aspects of the warm-season diel cycle during wet and dry conditions. First, for a wDry day, midday $\lambda E$ was enhanced by

**Table 2**
*Daytime and Nighttime Mean Statistics of Net Radiation $R_{net}$, Sensible Heat Flux H, and Latent Heat Flux $\lambda E$ for dDry and wDry Precipitation Conditions for the Warm Season for Years 1999–2003 and 2006–2014*

| | | | Daytime (10:00–14:00 MST) | | | Night (00:00–04:00 MST) | | | 2010 cumulative sums[a] | |
|---|---|---|---|---|---|---|---|---|---|---|
| Site or model | LAI | Variable | dDry | wDry | wDry-dDry | dDry | wDry | wDry-dDry | Total (MW $m^{-2}$) | Percent from US-NR1 (%) |
| US-NR1[b] | 3.8–4.2 | $R_{net}$ | 572.8 | 523.3 | −49.5 | −70.7 | −52.6 | 18.1 | 1,693.4 | 0 |
| | | $H$ | 270.5 | 197.1 | −73.4 | −48.7 | −53.8 | −5.1 | 693.0 | 0 |
| | | $\lambda E$ | 172.6 | 195.3 | **22.7** | 9.2 | 24.0 | **14.8** | **735.5** | 0 |
| US-Ho1[c] | ≈5.5 | $R_{net}$ | 471.5 | 460.3 | −11.2 | −37.3 | −28.2 | 9.1 | 1,353.9 | −20.0 |
| | | $H$ | 210.5 | 175.6 | −34.9 | −17.6 | −23.3 | −5.6 | 593.2 | −14.4 |
| | | $\lambda E$ | 169.4 | 189.7 | **20.3** | 1.4 | 1.4 | **0.02** | **646.0** | **−12.2** |
| A1 | 2 | $R_{net}$ | 549.7 | 509.6 | −40.0 | −68.9 | −56.9 | 12.0 | 1,538.8 | −9.1 |
| | | $H$ | 337.2 | 267.3 | −69.9 | −48.1 | −39.9 | 8.2 | 834.4 | 20.4 |
| | | $\lambda E$ | 132.6 | 169.0 | **36.4** | 9.7 | 15.6 | **5.9** | **616.9** | **−16.1** |
| A1 | 4 | $R_{net}$ | 557.9 | 514.3 | −43.7 | −64.2 | −53.2 | 11.0 | 1,593.5 | −5.9 |
| | | $H$ | 337.4 | 298.0 | −39.4 | −51.7 | −43.6 | 8.1 | 794.6 | 14.7 |
| | | $\lambda E$ | 160.8 | 163.2 | **2.4** | 9.4 | 12.6 | **3.1** | **719.5** | **−2.2** |
| A1 | 6 | $R_{net}$ | 561.9 | 517.1 | −44.8 | −62.1 | −51.7 | 10.4 | 1,620.1 | −4.3 |
| | | $H$ | 335.2 | 305.3 | −29.9 | −53.9 | −47.0 | 6.9 | 766.0 | 10.5 |
| | | $\lambda E$ | 178.6 | 170.8 | −7.8 | 9.6 | 12.9 | **3.3** | **763.2** | **3.8** |
| B0 | 4 | $R_{net}$ | 558.0 | 515.1 | −42.9 | −64.4 | −53.7 | 10.7 | 1,591.4 | −6.0 |
| | | $H$ | 335.9 | 286.1 | −49.8 | −51.8 | −43.4 | 8.5 | 801.7 | 15.7 |
| | | $\lambda E$ | 162.1 | 176.0 | **13.9** | 9.5 | 12.1 | **2.6** | **707.1** | **−3.9** |
| B1 | 4 | $R_{net}$ | 558.0 | 515.3 | −42.7 | −64.2 | −53.6 | 10.6 | 1,591.3 | −6.0 |
| | | $H$ | 335.8 | 282.9 | −53.0 | −52.0 | −43.5 | 8.4 | 797.5 | 15.1 |
| | | $\lambda E$ | 164.2 | 181.3 | **17.2** | 9.4 | 12.3 | **2.8** | **719.9** | **−2.1** |
| B2 | 4 | $R_{net}$ | 556.8 | 514.3 | −42.6 | −71.7 | −57.5 | 14.2 | 1,528.9 | −9.7 |
| | | $H$ | 341.7 | 285.7 | −56.0 | −65.3 | −51.3 | 14.0 | 714.0 | 3.0 |
| | | $\lambda E$ | 159.8 | 178.8 | **19.0** | 13.1 | 15.8 | **2.7** | **746.3** | **1.5** |
| C0 | 4 | $R_{net}$ | 557.2 | 514.2 | −43.0 | −72.7 | −58.5 | 14.2 | 1,524.3 | −10.0 |
| | | $H$ | 337.8 | 288.4 | −49.5 | −66.5 | −47.7 | 18.8 | 716.8 | 3.4 |
| | | $\lambda E$ | 162.5 | 174.7 | **12.2** | 13.3 | 11.0 | −2.3 | **733.4** | **−0.3** |
| D0 | 4 | $R_{net}$ | 558.2 | 514.4 | −43.8 | −53.5 | −47.2 | 6.3 | 1,654.3 | −2.3 |
| | | $H$ | 332.6 | 295.8 | −36.8 | −35.5 | −36.3 | −0.9 | 861.0 | 24.2 |
| | | $\lambda E$ | 162.5 | 163.2 | **0.7** | 7.8 | 13.3 | **5.5** | **709.2** | **−3.6** |
| D1 | 4 | $R_{net}$ | 556.7 | 513.4 | −43.2 | −71.7 | −57.1 | 14.5 | 1,531.0 | −9.6 |
| | | $H$ | 344.0 | 297.1 | −46.9 | −65.1 | −52.0 | 13.2 | 707.7 | 2.1 |
| | | $\lambda E$ | 157.6 | 166.3 | **8.7** | 12.8 | 16.6 | **3.8** | **755.6** | **2.7** |
| D2 | 4 | $R_{net}$ | 562.8 | 518.5 | −44.3 | −71.7 | −56.9 | 14.8 | 1,550.0 | −8.5 |
| | | $H$ | 357.2 | 314.4 | −42.8 | −66.2 | −51.9 | 14.3 | 741.7 | 7.0 |
| | | $\lambda E$ | 152.5 | 157.0 | **4.5** | 13.0 | 15.9 | **2.9** | **736.5** | **0.1** |
| D3 | 4 | $R_{net}$ | 556.5 | 513.3 | −43.2 | −76.6 | −59.5 | 17.1 | 1,508.1 | −10.9 |
| | | $H$ | 346.7 | 298.6 | −48.0 | −73.4 | −56.2 | 17.2 | 681.0 | −1.7 |
| | | $\lambda E$ | 156.4 | 165.8 | **9.4** | 14.3 | 17.5 | **3.2** | **759.3** | **3.2** |
| E0 | 4 | $R_{net}$ | 557.8 | 514.4 | −43.4 | −64.1 | −53.2 | 10.9 | 1,593.2 | −5.9 |
| | | $H$ | 337.9 | 295.2 | −42.6 | −51.8 | −43.8 | 8.0 | 791.7 | 14.2 |
| | | $\lambda E$ | 162.3 | 168.0 | **5.7** | 9.4 | 12.8 | **3.5** | **730.8** | **−0.6** |
| F0 | 4 | $R_{net}$ | 557.9 | 514.4 | −43.5 | −64.2 | −53.3 | 10.9 | 1,593.6 | −5.9 |
| | | $H$ | 338.4 | 294.9 | −43.5 | −52.2 | −44.5 | 7.7 | 785.5 | 13.3 |
| | | $\lambda E$ | 161.4 | 167.4 | **6.0** | 10.0 | 14.2 | **4.2** | **730.6** | **−0.7** |
| F1 | 4 | $R_{net}$ | 557.6 | 514.5 | −43.0 | −64.3 | −53.4 | 10.9 | 1,592.7 | −5.9 |
| | | $H$ | 342.0 | 290.6 | −51.4 | −52.2 | −44.7 | 7.5 | 777.7 | 12.2 |
| | | $\lambda E$ | 160.4 | 174.1 | **13.7** | 9.8 | 14.8 | **5.0** | **745.3** | **1.3** |
| F2 | 4 | $R_{net}$ | 555.9 | 513.1 | −42.8 | −72.0 | −57.3 | 14.7 | 1,529.9 | −9.7 |
| | | $H$ | 355.2 | 298.0 | −57.2 | −65.0 | −52.6 | 12.5 | 699.7 | 1.0 |
| | | $\lambda E$ | 148.9 | 166.9 | **18.0** | 12.9 | 18.7 | **5.8** | **765.1** | **4.0** |

**Table 2.** (continued)

| Site or model | LAI | Variable | Daytime (10:00–14:00 MST) dDry | wDry | wDry-dDry | Night (00:00–04:00 MST) dDry | wDry | wDry-dDry | 2010 cumulative sums[a] Total (MW m$^{-2}$) | Percent from US-NR1 (%) |
|---|---|---|---|---|---|---|---|---|---|---|
| G1 | 4 | $R_{net}$ | 562.7 | 519.2 | −43.5 | −71.9 | −57.3 | 14.6 | 1,547.6 | −8.6 |
| | | $H$ | 359.6 | 298.0 | −61.6 | −66.9 | −51.9 | 14.9 | 734.0 | 5.9 |
| | | $\lambda E$ | 152.4 | 175.7 | **23.4** | 13.7 | 17.0 | **3.3** | **742.0** | **0.9** |

*Note*. Years 2004 and 2005 were not used because the four-component radiometer on the US-NR1 tower was not available, which provided the incoming shortwave and longwave radiation used as input to drive CLM. At US-Ho1, statistics are from years 1996 to 2014. The CLM4.5 results are from US-NR1 for different configurations of the CLM4.5 software as shown by the alphanumeric code listed in column 1 and described in Table 1. Column 2 has the estimated leaf area index (LAI) for the flux sites or the LAI used by CLM4.5. All $R_{net}$, $H$, and $\lambda E$ daytime and nighttime values in the table have units W m$^{-2}$, and those in bold are emphasized within the text. The two right-hand columns show the cumulative sum of $R_{net}$, $H$, and $\lambda E$ over the 2010 warm season (units: MW m$^{-2}$) and the percent difference relative to the US-NR1 measurements, respectively.

[a]Cumulative sums of each variable for the warm season of 2010 (June–September) are shown along with the percentage difference relative to the US-NR1 tower measurements. The cumulative sums of the energy terms have units of megawatt (MW) per square meter of forest. [b]For US-NR1, the number of 30 min samples within each of the precipitation categories are dDry = 1,148, dWet = 177, wWet = 97, and wDry = 180. The CLM statistics are from the same time periods as US-NR1. [c]For US-Ho1, the number of 30 min samples within each of the precipitation categories are dDry = 1,029, dWet = 161, wWet = 50, and wDry = 214.

≈40 W m$^{-2}$ relative to dry conditions, with a concomitant reduction in sensible heat flux $H$. Second, nocturnal $\lambda E$ increased from ≈10 W m$^{-2}$ in dry conditions to over 20 W m$^{-2}$ in wet conditions. Based on these observations from the measured fluxes, we evaluate CLM4.5 using the following statistics: (1) calculating the mean difference in midday composite energy fluxes on a wDry day compared to a dDry day and (2) taking the difference in nocturnal energy fluxes between 0 and 4 LST for a dDry period compared to a wDry period. Using $\lambda E$ as an example, these statistics will be designated as "wDry-dDry $\lambda E$" in our discussion. These simple statistics will be applied to both the US-NR1 and US-Ho1 measurements and CLM4.5 model output. By using the difference statistics, we are not explicitly comparing the mean values of the observed and CLM4.5 fluxes, but instead checking that the model and observations are responding to precipitation events in a consistent way.

Air and soil temperatures are readily measured in the field and calculated by CLM4.5, making them useful to evaluate the model performance. At US-NR1, three levels of aspirated air temperature and 11 levels of thermocouple air temperature from near the ground to twice canopy height were measured (Burns et al., 2015). We compare these tower observations with various CLM4.5 temperatures, which are canopy surface temperature $T_v$, canopy airspace temperature $T_s$, the "2 m" level air temperature $T_{2m}$, and ground surface $T_g$ and subsurface soil temperatures $T_{soil}$. Because CLM4.5 is a simple single-leaf model, temperatures such as $T_s$ and $T_{2m}$ are attempting to represent an average temperature from many locations where the true temperature may widely differ (e.g., shady versus sunny portions of the canopy). Therefore, the precise vertical location of $T_v$, $T_s$, and $T_{2m}$ can be a bit vague. In the CLM4.5 manual $T_{2m}$ is defined as being "2 m above the apparent sink for sensible heat" which is defined by the roughness length for heat and displacement height (Oleson et al., 2013). Since $T_{2m}$ and $T_s$ are usually only separated by an offset, we will often only show $T_s$ which should be comparable with air temperature observations within the canopy (at US-NR1, these are the thermocouples or aspirated temperature sensors at 2 and 8 m).

#### 2.3.4. Additional Details

The dDry conditions are likely to provide the most robust comparison for the following reasons: (1) they are the most common precipitation state with approximately 1,148 days (or over 3 years worth of 30 min time periods) available for analysis which provides good statistics and (2) the gap-filling of the fluxes due to sensor problems caused by precipitation are at a minimum in dDry and wDry conditions. For a list of the problems that precipitation causes with eddy-covariance measurements, see van Dijk et al. (2015).

Our analysis examines the sensitivity of CLM fluxes and temperatures to changing certain variables or parameters within CLM4.5, using the nomenclature and alphanumeric descriptions in Table 1. For example, "CLM4.5 A1" will be considered the default configuration of CLM4.5. The leading letter describes changes to a specific variable (A is default, B is related to $f_{wet}^{max}$, C is related to $u_*$, and so on). Unless specified otherwise, the CLM4.5 results in our plots are shown as closed or filled symbols and the tower observations are shown as open circles.

## 3. Results and Discussion

### 3.1. Net Radiation and Turbulent Energy Fluxes

After each day was organized into the precipitation categories described in section 2.3.1, the mean diel cycle of net radiation, the turbulent energy fluxes, and precipitation are plotted side-by-side based on the precipitation state for a given day (Figure 1). As one would expect, a majority of the rain occurred during dWet and wWet days (Figure 1d) when clouds increased and midday net radiation was reduced (Figure 1a). Our analysis is focused on two main features of Figure 1: (i) in wDry conditions midday $\lambda E$ was enhanced by around 40 W $m^{-2}$ compared to dDry conditions with a concomitant reduction in midday sensible heat flux (green arrows in Figures 1b and 1c) and (ii) at night, in wet conditions, latent heat flux was enhanced by about 15 W $m^{-2}$ relative to dDry conditions (highlighted by the blue arrows in Figure 1c). Numerical values of dDry and wDry $\lambda E$ and $H$ (as well as wDry-dDry) are listed in Table 2, with other aspects of the effect of precipitation on the composite diel cycle at US-NR1 discussed in Burns et al. (2015).

In Figure 2, the CLM4.5 A1 net radiative and turbulent fluxes are compared with the measurements. Because CLM4.5 used the measured incoming shortwave and longwave radiation as input to the model, it is to be expected that CLM4.5 net radiation agrees well with the observations. In general, during daytime, the CLM4.5 sensible heat flux was larger than the observations by anywhere from 50 to 100 W $m^{-2}$ (Figure 2b) whereas daytime CLM4.5 latent heat flux was similar or smaller than measured $\lambda E$ (Figure 2c). With the exception of friction velocity, the variability or SD-Bin of the measured fluxes and CLM4.5 were of similar magnitude (supporting information Figure S1). However, if we focus on the two items related to $\lambda E$ highlighted in the previous paragraph, we found that CLM did not properly reproduce either the increase in $\lambda E$ on wDry days or the enhanced latent heat flux at night in wet conditions. The CLM4.5 latent heat flux during midday and at night on wDry days was only slightly larger than $\lambda E$ during those same periods on dDry days (for numerical values, see the CLM4.5 A1 entry in Table 2).

### 3.2. Components of Latent Heat Flux in CLM4.5

Latent heat flux is a combination of transpiration $\lambda E_v^t$, and evaporation from the ground $\lambda E_g$ and vegetation/canopy $\lambda E_v^w$ surfaces. The component parts of CLM4.5 $\lambda E$ at three different LAI values are shown in Figure 3. As LAI was increased, the components were affected as follows: (1) transpiration increased, (2) canopy evaporation increased slightly, and (3) ground evaporation decreased significantly. For all three LAI values in Figure 3, CLM transpiration on a wDry day was similar to that of a dDry day. Therefore, if CLM is going to reproduce the enhanced $\lambda E$ during a wDry day observed at US-NR1, this "enhancement" needs to come from the canopy and ground evaporation. For LAI = 2, we can see that midday $\lambda E$ on a wDry day was larger than on a dDry day due to an increase in ground evaporation within a relatively more open forest (Figure 3a). The increase in wDry $\lambda E$ qualitatively matches the US-NR1 observations shown in Figure 3b, top, and we will discuss more about the LAI = 2 results in section 3.3.

Next, we consider $\lambda E$ on the afternoon of wet (dWet and wWet) days in Figure 3. At these times, US-NR1 $\lambda E$ was decreased relative to dDry $\lambda E$. For CLM, the reduction in $\lambda E$ on the afternoon of wet days became larger as LAI increased; however, even for LAI =6, the reduction was not as large as the US-NR1 observations. In contrast, the reduction of the CLM transpiration on wet-day afternoons looks qualitatively similar to the $\lambda E$ observations. The lack of diel symmetry in CLM $\lambda E$ implies that the asymmetry in transpiration was offset by higher values of canopy evaporation on wet afternoons (soil evaporation being symmetric about midday). This suggests that the timing and/or magnitude of the CLM canopy evaporation term was problematic.

Another observation from Figure 3 is that at night both the canopy and ground evaporation terms were small (less than 5 W $m^{-2}$), regardless of whether it was a dry or wet period. Soil evaporation is thought to have two stages: one when soil moisture is high and atmospheric demand controls evaporation, and a second stage where the soil surface is relatively dry and diffusion of water vapor through the soil controls surface evaporation (Brutsaert, 1982). For a crop, it has been shown that soil evaporation doubles when irrigation exists and nighttime evaporation can account for over 10% of daily $\lambda E$ (Tolk et al., 2006). In Figure 3, CLM ground evaporation appears to be primarily controlled by LAI and there is little evidence that the existence of liquid water was playing a role in modifying the soil evaporation, especially at night. Furthermore, if soil evaporation is expected to be higher when the soil is wet, one would not expect near-perfect symmetry (around noon) on a wDry day.

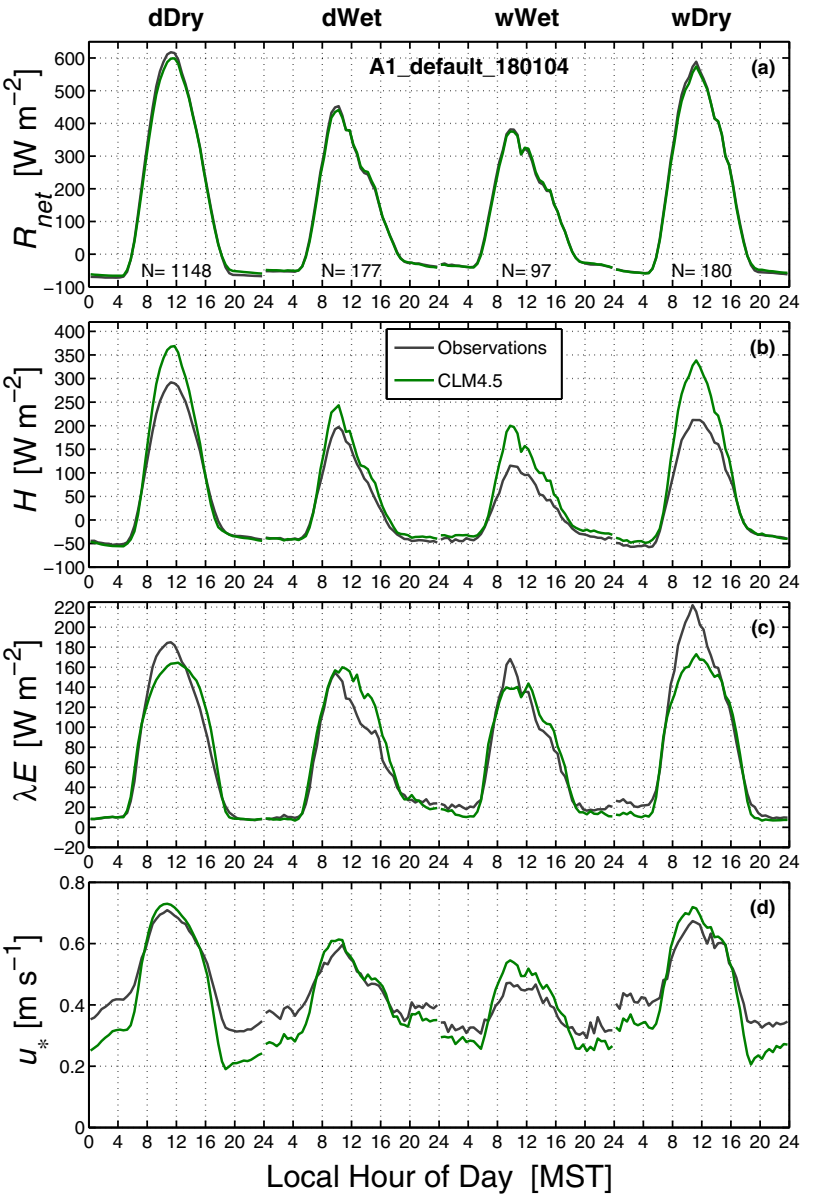


**Figure 2.** Similar to Figure 1, but a comparison of the observations and CLM4.5 model output for (a) net radiation $R_{net}$, (b) sensible heat flux $H$, (c) latent heat flux $\lambda E$, and (d) friction velocity $u_*$. The legend in Figure 2b applies to all figures. The CLM results use the CLM4.5 A1 (default) configuration with a leaf area index (LAI) of 4 (Table 1).

From Figure 3b, we can roughly estimate that the CLM canopy and ground evaporation terms both reached maximum values during midday of wet days, with values of 50–60 and 10 W m$^{-2}$, respectively. CLM $\lambda E$ peaked at similar times, at a value of around 150 W m$^{-2}$. These values suggest that CLM canopy evaporation and ground evaporation were no higher than 36% and 6% of the total $\lambda E$, respectively. In a pine-spruce forest of similar LAI to that of US-NR1, Grelle et al. (1997) found that the canopy and soil evaporation components of total $\lambda E$ accumulated over a growing season were ≈20% and 15%, respectively. Based on these numbers, canopy and ground evaporation should have similar magnitudes, and the CLM ground evaporation seems low.

In the observations, we have assumed that transpiration at night is small. CLM4.5 allows for a small level of nocturnal transpiration ($\lambda E_v^t$ on the order of 5 W m$^{-2}$), and we will revisit this topic in section 3.8.1. The separation of nocturnal $\lambda E$ into transpiration and evaporation is a complicated problem (e.g., Novick et al., 2009), and for more discussion about the possibility of nocturnal transpiration at the US-NR1 site see

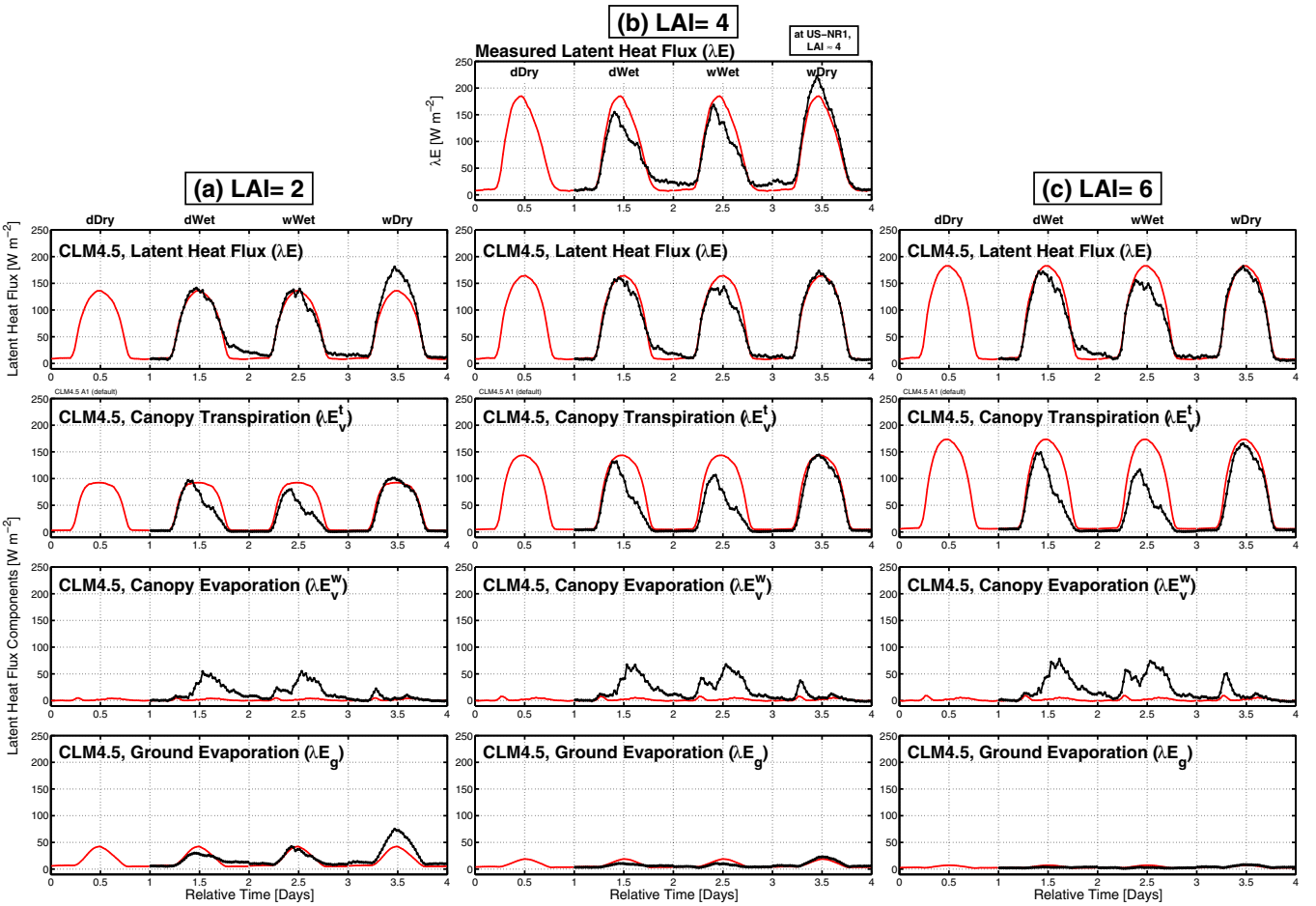


**Figure 3.** The mean diel cycle of latent heat flux $\lambda E$ separated into dDry, dWet, wWet, and wDry conditions for (a) leaf area index LAI = 2, (b) LAI = 4, and (c) LAI = 6. The red line in each figure is the mean diel cycle for dDry conditions which is repeated for ease of comparison to the results from dWet, wWet, and wDry conditions. (top, middle) $\lambda E$ measured at the US-NR1 tower which has an LAI of around 4. Below that are the CLM4.5 model output which are (from the second to bottom row): total latent heat flux $\lambda E$; canopy transpiration $\lambda E_v^t$; canopy evaporation $\lambda E_v^w$; and ground evaporation $\lambda E_g$. Other than changes to LAI, CLM uses the CLM4.5 A1 (default) configuration.

Turnipseed et al. (2009). We hypothesize that the topographically induced nocturnal slope flow at US-NR1 resulted in a higher-than-expected nocturnal ground evaporation component (to be discussed in section 4.4).

### 3.3. Sensitivity of CLM4.5 Latent Heat Flux and Temperature to Leaf Area Index (LAI)

As LAI was increased from 2 to 6, we found that dDry midday latent heat flux increased from ≈133 to 179 W m$^{-2}$, while sensible heat flux stayed approximately the same (Figure 4a1 and Table 2). For the midday wDry-dDry fluxes, net radiation was nearly constant with changing LAI, while the $\lambda E$ difference became smaller and went slightly negative as LAI increased (Figure 4b1). This means that the enhancement of $\lambda E$ at midday on a wDry day became smaller as LAI was increased (the observations at the US-NR1 tower suggest that wDry-dDry $\lambda E$ should be 22 W m$^{-2}$). In Figure 4b1, one can follow the blue dashed line for the observations and see it intersects the CLM wDry-dDry $\lambda E$ at a value of LAI ≈ 2.5. As discussed in the previous section, increased CLM wDry $\lambda E$ for LAI = 2 was due to increased ground evaporation. While it makes sense that reducing LAI would lead to enhanced midday wDry $\lambda E$, LAI is a fairly well-constrained variable, and it does not seem realistic to use such a low LAI value for the US-NR1 site. Therefore, we reject the possibility that LAI explains the mismatch in wDry-dDry $\lambda E$ between CLM and the observations.

The midday CLM4.5 canopy air temperature $T_s$ was unaffected by increasing LAI, but vegetation surface temperature $T_v$ decreased by around 2°C and $T_g$ decreased by 8°C (Figure 4c1). The dramatic decrease in ground surface temperature was, presumably, due to increased shading of the soil surfaces as LAI increased.

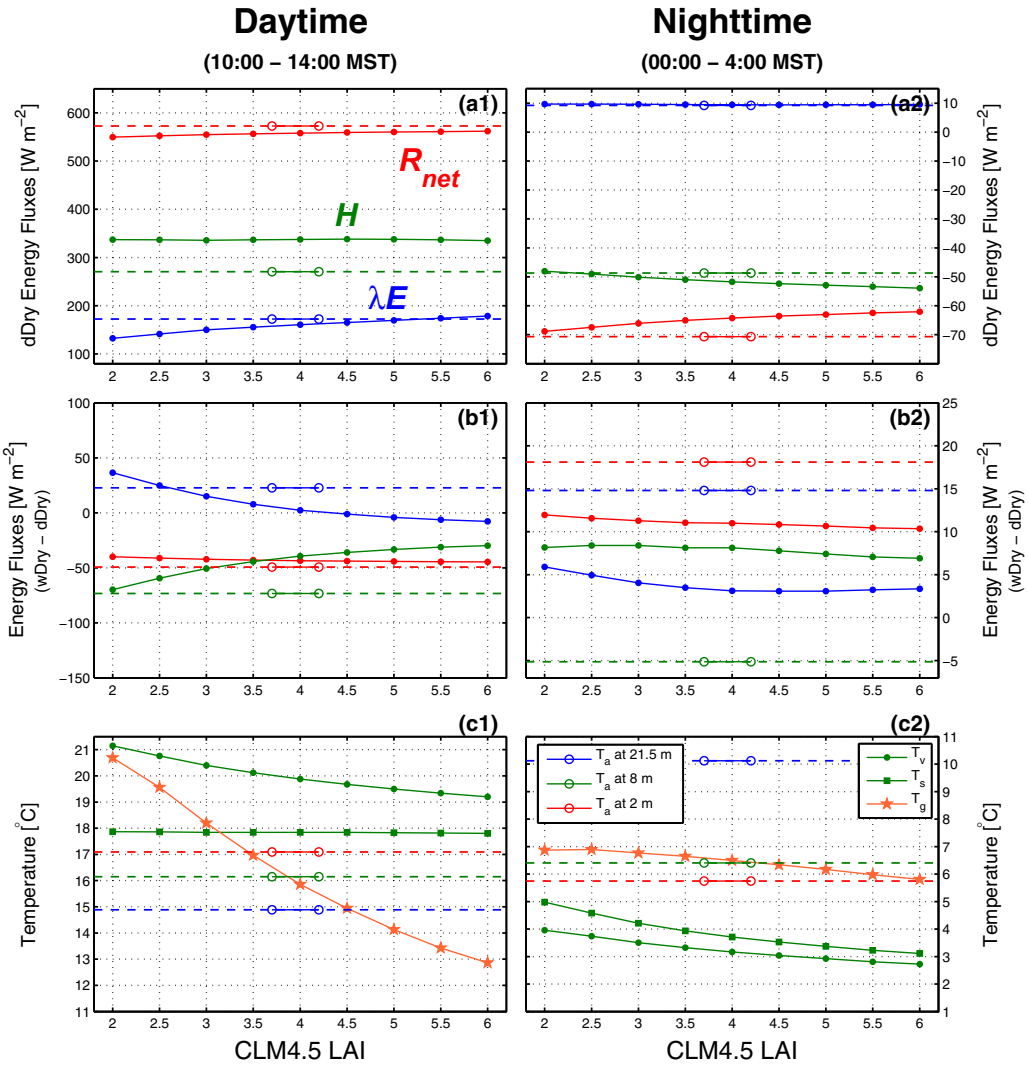


**Figure 4.** (a1, b1) Daytime and (a2, b2) nighttime energy fluxes versus CLM4.5 leaf area index (LAI) as it varies from 2 to 6. (top) The mean values for dDry conditions and (middle) the mean differences between wDry and dDry conditions where the variables shown are net radiation $R_{net}$ (red), sensible heat flux $H$ (green), and latent heat flux $\lambda E$ (blue). The solid lines with filled symbols are the CLM4.5 output, while the shorter lines with open circles are the US-NR1 above-canopy tower observations over an approximate range of the site LAI (3.7–4.2). (c1, c2) The US-NR1 observed air temperature $T_a$ and the effect of varying LAI on CLM canopy surface $T_v$, canopy air $T_s$ and ground $T_g$ temperatures are shown (see legends). The CLM results use the CLM4.5 A1 (default) configuration (Table 1).

The decrease in CLM $T_g$ resulted in a smaller soil heat flux to keep the surface energy budget balanced (results not shown).

At night, the CLM4.5 dDry latent heat flux was very close to the observations (on the order of 10 W m$^{-2}$) and insensitive to LAI changes, whereas net radiation decreased in magnitude as LAI increased and sensible heat flux increased in magnitude to compensate for the $R_{net}$ changes (Figure 4a2). For all the LAI values considered, the CLM4.5 nocturnal wDry-dDry latent heat flux was less than 6 W m$^{-2}$, much less than the observed value of 15 W m$^{-2}$ (Figure 4b2). This suggests that LAI does not play a significant role in controlling the nocturnal latent heat flux (in wet conditions). All the CLM4.5 nighttime temperatures decreased by around 1–2°C as LAI was increased (Figure 4c2).

### 3.4. Sensitivity of CLM4.5 Latent Heat Flux to Maximum Leaf Wetted Fraction

When water is present on the canopy, the *maximum leaf wetted fraction* $f_{wet}^{max}$ limits the area of the leaf surface that is wet. A larger $f_{wet}^{max}$ value decreases the portion of the canopy undergoing transpiration and

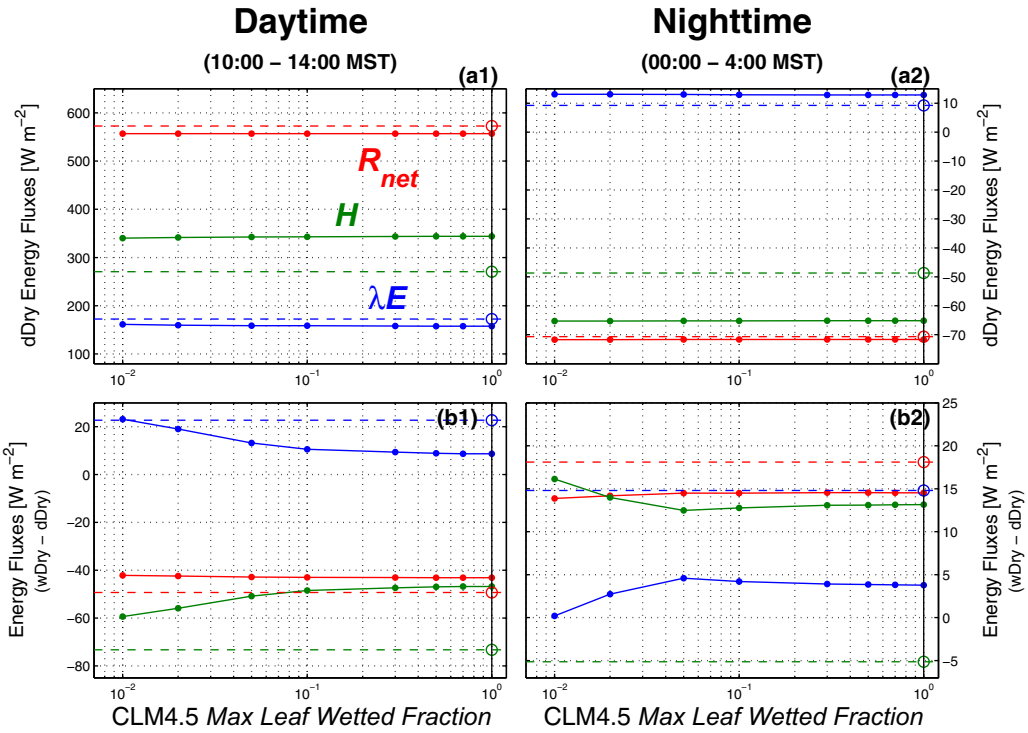


**Figure 5.** (a1, b1) Daytime and (a2, b2) nighttime energy fluxes versus changes to the CLM4.5 *maximum leaf wetted fraction* $f_{wet}^{max}$ as it varies from 0.01 to 1 (the CLM4.5 default value is 1). (top) The mean values for dDry conditions and (bottom) the mean differences between wDry and dDry conditions where the variables shown are net radiation $R_{net}$ (red), sensible heat flux $H$ (green), and latent heat flux $\lambda E$ (blue). The solid lines with filled symbols are the CLM4.5 output, while the horizontal dashed lines are the US-NR1 observations with an open circle (and vertical black line) placed at the default $f_{wet}^{max}$ value. The CLM results use the CLM4.5 B2 configuration (Table 1).

increases the direct evaporation of canopy water. For $f_{wet}^{max}=1$, the entire leaf is covered in water, which is the CLM4.5 default value. This default setting is unlikely to be appropriate for needleleaf conifers, where rainwater accumulates at the tips of the needles that act as drip points (Moors, 2012).

For $f_{wet}^{max}$ varied between 0.01 and 1, the CLM4.5 dDry fluxes were only minimally affected, as would be expected in dry conditions (Figures 5a1 and 5a2). However, when $f_{wet}^{max}$ was smaller than 0.05, it had a significant effect on the wDry-dDry $\lambda E$ and $H$ fluxes. For the midday wDry-dDry $\lambda E$ difference, the two smallest values of $f_{wet}^{max}$ (0.01 and 0.02) approached the wDry-dDry $\lambda E$ difference of the US-NR1 observations (Figure 5b1); however, these values also tended to decrease the nocturnal wDry-dDry $\lambda E$ difference toward zero (Figure 5b2). As a compromise, we examined the effect of setting $f_{wet}^{max}$ to 0.02 in our analysis (CLM4.5 B0, B1, and B2 in Table 1).

After setting $f_{wet}^{max}$ to 0.02, CLM midday $\lambda E$ in wDry conditions (Figure 6a) looked qualitatively similar to observed wDry $\lambda E$ (Figure 3b, top). Furthermore, CLM $\lambda E$ on the afternoon of wet days, was reduced (relative to dDry $\lambda E$), similar to the observations. Transpiration and soil evaporation were relatively unchanged by decreasing $f_{wet}^{max}$, but the canopy evaporation term was smoother and decreased in magnitude, especially during the afternoon (Figure 6a). Decreasing $f_{wet}^{max}$ does not change the amount of intercepted water, but it does cause the intercepted water to evaporate at a slower rate, making it more likely for the water to build up in the canopy and drip to the ground (rather than evaporate to the atmosphere).

A good example of the effect of decreasing $f_{wet}^{max}$ on the $\lambda E$ components can be seen in the wDry diel composite shown in Figure 6c. With CLM4.5 A1, there was a sharp increase in the canopy evaporation term at sunrise from near zero up to 40 W m$^{-2}$ which only lasted a few hours (between around 6:00 and 8:00 MST); in contrast, for CLM4.5 B0, the canopy evaporation term peaked at around 9:00 MST with a value of 40

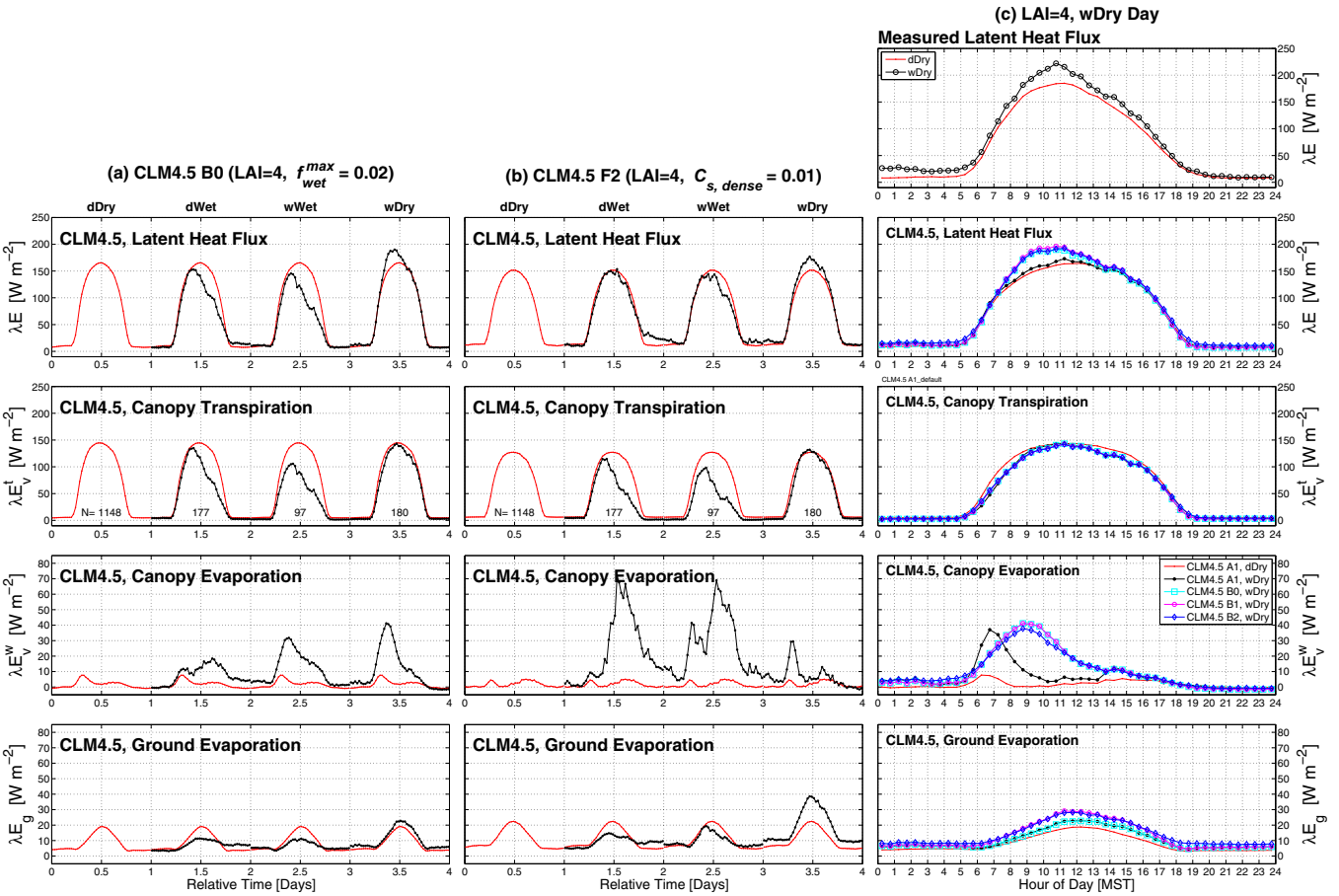


**Figure 6.** Components of the latent heat flux for (a) CLM4.5 using *maximum leaf wetted fraction* $f_{wet}^{max} = 0.02$ (CLM4.5 B0), (b) CLM4.5 with the subcanopy turbulent exchange coefficient $C_{s,dense} = 0.01$ (CLM4.5 F2), and (c) the results for a wDry day for the default settings (CLM4.5 A1) along with different cases of $f_{wet}^{max}$=0.02 as listed in the legend. A detailed description of each CLM4.5 alphanumeric configuration is in Table 1. For Figures 6a and 6b, the mean diel cycles are separated into dDry, dWet, wWet, and wDry conditions where the red line in each figure is the mean diel cycle for dDry conditions which is repeated for ease of comparison to the results from dWet, wWet, and wDry conditions. CLM4.5 $\lambda E$ is broken down into individual components which are (from top to bottom row): total latent heat flux $\lambda E$; canopy transpiration $\lambda E_v^t$; canopy evaporation $\lambda E_v^w$; and ground evaporation $\lambda E_g$. In Figure 6c, US-NR1 observed $\lambda E$ is shown in the top figure.

W m$^{-2}$ and the evaporation was spread over a much longer time period, between 6:00 and 13:00 MST. The other CLM4.5 configurations shown in Figure 6c (B1 and B2) will be discussed later, but the important point is that these configurations are second-order effects while the change to $f_{wet}^{max}$ presents a fundamental change to the nature of CLM canopy evaporation. To extend this knowledge further, better knowledge of the true canopy evaporation from the forest at US-NR1 would be required.

A final comment on Figure 6a: it is curious that the midday ground evaporation during dWet, wWet, and wDry conditions was either smaller or only slightly larger than that in dDry conditions. This is suggestive that $R_{net}$ plays a dominant role in controlling the CLM ground evaporation, as opposed to the availability of liquid water. One would expect that an important factor controlling the CLM ground evaporation term is the subcanopy turbulent transport, which will be discussed in section 3.8.

### 3.5. Atmospheric Turbulence and Latent Heat Flux

#### 3.5.1. Above-Canopy Friction Velocity

Mechanical turbulence (characterized by the friction velocity $u_*$) plays a crucial role in the transport of water vapor between the forest and the atmosphere. At US-NR1, $u_*$ generally follows a similar pattern to wind speed at night; however, during the daytime, the buoyancy generated by surface heating enhances $u_*$ relative to nocturnal values (Burns et al., 2015). Observed $u_*$ generally agrees well with CLM $u_*$ during midday, but at night we found that observed nocturnal $u_*$ was at around 0.4 m s$^{-1}$ while the CLM $u_*$ was closer to 0.3 m s$^{-1}$ (Figure 2d).

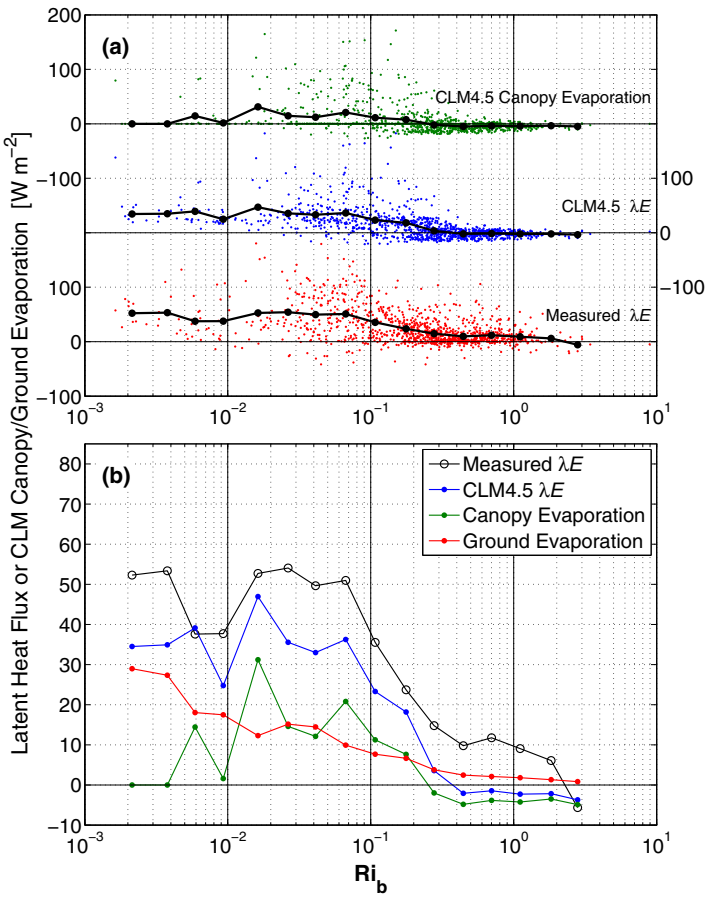


**Figure 7.** The US-NR1 and CLM4.5 latent heat flux $\lambda E$ and CLM4.5 canopy evaporation $\lambda E_v^w$ versus the bulk Richardson number $Ri_b$ from wDry periods between midnight and 4:00 MST. (a) All the 30 min values including an $Ri_b$-binned average of the 30 min data are shown. (b) The binned averages from Figure 7a are shown along with the CLM4.5 ground evaporation term as described in the legend. CLM results are from the CLM4.5 A1 configuration.

Another way to look at this issue is to examine how CLM and observed $u_*$ vary with bulk Richardson number $Ri_b$ (supporting information Figure S2). In general, it appears that CLM $u_*$ has a low-bias relative to the observed $u_*$ of around 0.1 m $s^{-1}$. Many flux observations sites show a similar $u_*$ bias with CLM4.5 (e.g., Bonan et al., 2017). Because $u_*$ is such an important variable, we circumvented this issue by using observed $u_*$ as an input to CLM4.5 (see Table 1 for specific configurations). In general, using observed $u_*$ increased the magnitude of the nocturnal fluxes (as one would expect). A more quantitative examination on the effect of using observed $u_*$ is in section 3.7.3.

#### 3.5.2. Atmospheric Stability Effects on Nocturnal Latent Heat Flux

We used the bulk Richardson number $Ri_b$ to examine how modeled and measured $\lambda E$ behaved in strongly stable conditions (Figure 7). Here we observe that on wDry days the magnitude of $\lambda E$ was reduced in strongly stable conditions (i.e., $Ri_b > 0.2$). In these strongly stable conditions, CLM $\lambda E$ had many negative 30 min periods, which suggests that there was net condensation on the canopy (not net evaporation). Based on the US-NR1 observations, net condensation ($\lambda E < 0$) was rare (Figure 7a). This becomes more apparent when looking at the $Ri_b$-binned averages in Figure 7b. In strongly stable conditions, even though the ground evaporation term was slightly positive, the canopy evaporation term was negative, which led to CLM $\lambda E$ being slightly negative (on average). One explanation for condensation to dominate the CLM canopy evaporation term would be if the the CLM canopy surface temperature dropped below the dewpoint temperature. A comparison of observed and CLM temperatures is our next topic of discussion.

### 3.6. Vegetation, Air, and Soil Temperature

At midday in dDry conditions, the air within the canopy and near the ground at the US-NR1 site was fairly uniform in temperature and, on average, was ≈1–2°C warmer than the air just-above the forest (Figure 8a). This compares fairly well with the midday CLM4.5 A1 temperatures. However, the nighttime temperatures show much less agreement (Figure 8b). For CLM4.5 A1 at night, the canopy surface temperature $T_v$ was around 3°C colder than the ground surface and about 0.5°C colder than the canopy air temperature $T_s$. Therefore, CLM considers the air within the canopy the coldest location within the forest. In contrast, the US-NR1 observations suggest that the coldest air was just-above the ground surface, and near-ground $T_a$ was only ≈1°C cooler than $T_{soil}$. In a study at an evergreen forest using a thermal IR camera, Kim et al. (2016) showed that the nocturnal canopy skin temperature was typically ≈2°C colder than the nearby air temperature. Recent work with IR cameras at US-NR1 have shown that the nighttime canopy IR and air temperatures are, on average, within about 1°C of each other (Aubrecht et al., 2016; Bowling et al., 2018). This seems similar to CLM $T_s - T_v$; however, the vertical temperature profiles in Figure 8a clearly reveal that CLM $T_s$ was over 2°C colder than any level of the US-NR1 tower observations. If CLM was performing correctly, we would expect $T_s$ to be closer to observed subcanopy $T_a$.

For nocturnal air temperatures plotted versus $Ri_b$ with CLM4.5 A1 (Figure 9b1), the stronger the stability, the colder the CLM vegetation and canopy airspace temperatures became, such that $T_s - T_g$ was on the order of −6°C for the highest stabilities (Figure 9b2). In contrast, US-NR1 $T_a$ measured within the subcanopy airspace appeared to reach a limit within strongly stable conditions, as shown by the 2 and 8 m $T_a$ curves leveling off at ≈4°C for $Ri_b > 0.8$ (Figure 9a1). Presumably, this was due to the drainage flow forming in strongly stable conditions which increased turbulent mixing of (warmer) air aloft with air near the ground. The cold bias in CLM canopy temperatures and small values of friction velocity appear to be symptoms of runaway cooling, as discussed in the Introduction. In section 3.7.3, we will discuss the effect of using observed $u_*$ on the CLM temperatures.

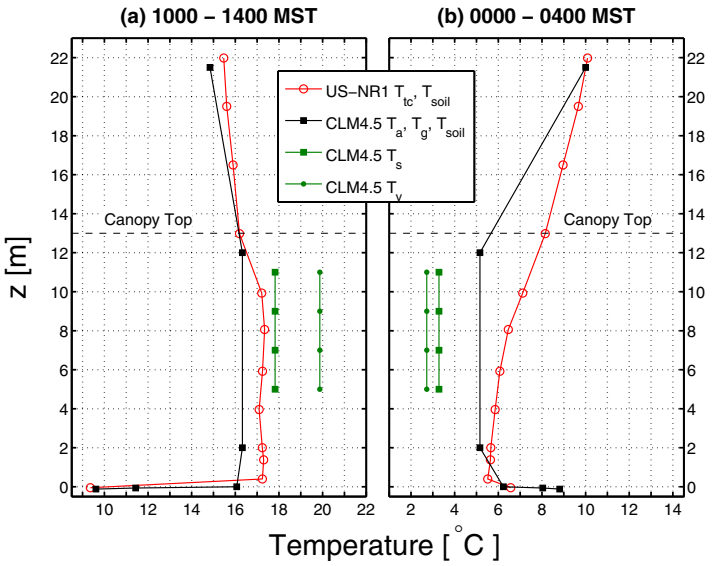


**Figure 8.** Average (a) daytime and (b) nighttime vertical temperature profiles in dDry conditions during the warm season for years 2006–2012. As shown in the legend, the US-NR1 air temperature $T_a$ profile is from 11 levels of thermocouples $T_{tc}$ and soil temperature at −5 cm depth. The CLM model includes temperature estimates of canopy vegetation $T_v$, the canopy airspace $T_s$, and a 2 m air temperature $T_{2m}$ defined as 2 m above the apparent sink for sensible heat (Oleson et al., 2013). We show $T_{2m}$ as the temperature between 2 m $\leq z \leq$ 12 m, and $T_v$ and $T_s$ are shown between 5 m $\leq z \leq$ 11 m. The approximate canopy top is shown as a horizontal dashed line at $z =$ 13 m. CLM results are from the CLM4.5 A1 (default) configuration (Table 1).

In strongly stable conditions, the dewpoint temperature $T_d$ measured at the US-NR1 site was ≈–2°C, or 6°C below the air temperature (Figure 9a1). The magnitude of this difference was fairly close to the CLM vegetation cold temperature bias, which suggests that the bias was likely contributing to condensation forming on the canopy in CLM (i.e., leading to $\lambda E_v^w < 0$).

### 3.7. Above-Canopy Turbulent Exchange in CLM4.5

CLM4.5 uses Monin-Obukhov Similarity Theory (MOST) to calculate the turbulent fluxes between the atmosphere and the atmospheric surface layer, where the surface-layer fluxes approximate those near the ground (e.g., Businger et al., 1971; Foken, 2006; Panofsky & Dutton, 1984). To model the turbulent fluxes, MOST utilizes the so-called universal similarity functions.

#### 3.7.1. Universal Similarity Functions

One of the primary tenets of MOST is that, under specified conditions, there exists universal functions ($\phi_m$, $\phi_h$, and $\phi_w$) that model the vertical gradients of wind, temperature and humidity, as

$$\phi_m(\zeta) = \frac{\kappa(z-d)}{u_*}\frac{\partial U}{\partial z}, \tag{2}$$

$$\phi_h(\zeta) = \frac{\kappa(z-d)}{\theta_*}\frac{\partial \theta}{\partial z}, \tag{3}$$

$$\phi_w(\zeta) = \frac{\kappa(z-d)}{q_*}\frac{\partial q}{\partial z}, \tag{4}$$

where $\kappa$ is the von Karman constant, $z$ is the height above the ground, $d$ is the zero-plane displacement height, and other variables are defined in Table B1. The universal functions are a function of only a single variable—the dimensionless stability parameter $\zeta = (z-d)/L$, where $L$ is the Obukhov length (see Table B1 for details). After the form of the universal functions are empirically determined, they can be numerically integrated and the changes in horizontal wind speed and scalars with height in the surface layer can be calculated. Additional details can be found in any standard boundary layer or micrometeorology textbook (e.g., Foken, 2008; Kaimal & Finnigan, 1994); for our purposes, we highlight that stability $\zeta$ and mechanical turbulence (represented by the friction velocity, $u_*$) are two of the primary variables controlling turbulent exchange which affects the degree of mixing that occurs between the ground surface and atmosphere. The fact that $u_*$ is part of $L$ is the so-called self-correlation issue with MOST (e.g., Baas et al., 2006; Moene & Van Dam, 2014). Another possible issue using MOST over a forest exists if the tower measurement level is too close to the surface roughness elements (i.e., within the so-called roughness sublayer RSL), then the standard MOST universal functions can introduce a bias to the modeled canopy-atmosphere exchanges (e.g., Harman & Finnigan, 2007, 2008).

In Table 3, we list the universal functions used in CLM4.5 separated into different stability regimes. In stable conditions, the universal functions for momentum $\phi_m$, heat $\phi_h$, and moisture $\phi_w$ are identical. In unstable conditions, $\phi_h$ and $\phi_w$ are still identical, but the form of $\phi_m$ changes and occurs over a different stability range. The accuracy of the universal functions is typically on the order of 10–20%, with larger uncertainty in strongly stable (i.e., z-less scaling) and unstable (i.e., free convection) conditions (Foken, 2008). In CLM4.5, the MOST equations are solved iteratively until a convergent solution is achieved (based on changes in vegetation temperature and transpiration being below a certain limit, or after 40 iterations have been carried out). Full details of the CLM4.5 methodology are provided in Oleson et al. (2013).

Over the years, many different forms of the universal functions have been proposed (see Foken, 2008 for a list of examples). It is natural to wonder how much of an effect the choice of universal function has on the model results. The universal functions that we consider within our study are listed in Table 4. In Figure 10, we show the CLM4.5 universal functions (based on the work by Zeng et al., 1998) along with the classical one from Högström (1988) versus $\zeta$. In this figure, we include the frequency distributions of $\zeta$ measured at 21.5 m on the US-NR1 tower—as one would expect, nocturnal conditions are typically stable (94% of the

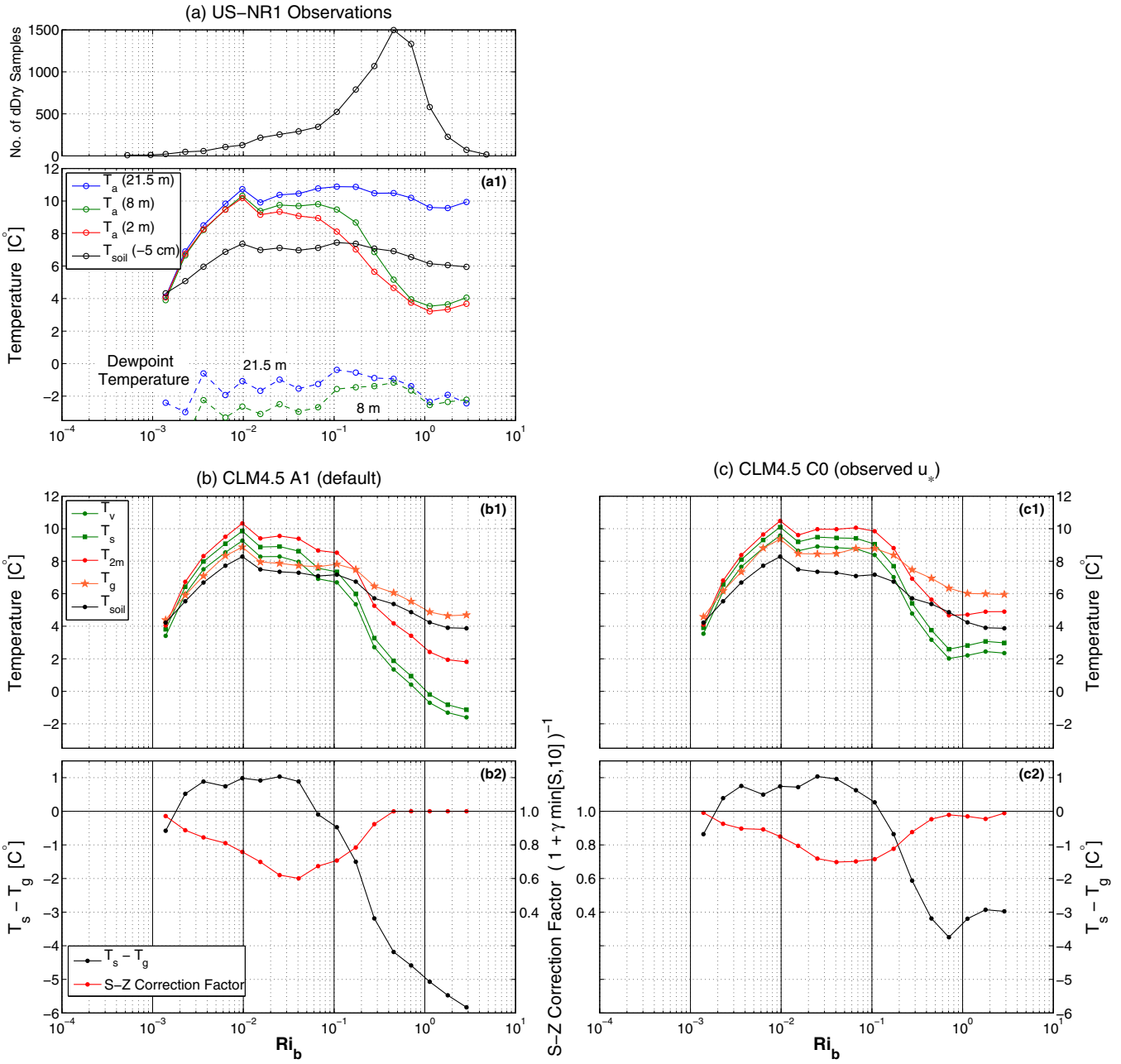


**Figure 9.** (a1) US-NR1 observed air $T_a$, dewpoint $T_d$, and soil $T_{soil}$ temperatures, (b1) CLM4.5 A1 (default configuration) temperatures, and (c1) CLM4.5 C0 (CLM using observed friction velocity $u_*$) temperatures versus the bulk Richardson number $Ri_b$. The legends in Figure 9b also applies to Figure 9c, where the CLM temperatures shown are: canopy vegetation temperature $T_v$, canopy airspace temperature $T_s$, "2 m" air temperature $T_{2m}$, ground surface temperature $T_g$, and $T_{soil}$ at −6.2 cm depth. In Figure 9a, the top figure shows the number of 30 min samples within each $Ri_b$ bin, and only results with at least 20 samples in a bin are presented. (b2, c2) The CLM4.5 $T_s - T_g$ difference versus the bulk Richardson number $Ri_b$ are shown in black along with the S-Z correction factor proposed by Sakaguchi and Zeng (2009) in red. For $T_s - T_g > 0$, the S-Z correction (based on the stability parameter $S$ with $\gamma = 0.5$) is intended to reduce the value of the subcanopy turbulent transfer coefficient $C_{s,dense}$. The mean of the S-Z correction factor uses the $y$ axis between Figures b2 and c2. These data are from dDry periods between midnight and 4:00 MST.

nighttime periods have $\zeta > 0$). Högström (1988) is only defined up to $\zeta = 1$ which is near the peak of the nocturnal $\zeta$ frequency distribution. For $\zeta > 1$, the form of the universal function is not well understood, and the default CLM4.5 form for $\phi$ suggests it should increase sharply. However, the work by Handorf et al. (1999) and others suggest that $\phi$ should be capped at a fixed value within the strongly stable regime. One of our objectives is to test which formulation of $\phi$ leads to CLM4.5 fluxes that agree best with the US-NR1 measured fluxes. On the unstable side ($\zeta < 0$), the differences between the CLM4.5 and Högström (1988) $\phi$ functions are less dramatic (Figures 10a2 and 10a3).

**Table 3**
*Universal Functions for Momentum $\phi_m$, Heat $\phi_h$, and Moisture $\phi_w$ Used in CLM4.5 Listed by Stability Range Based on the Stability Parameter, $\zeta$*

| Stability range | CLM4.5 manual equation no. | Universal functions for momentum, heat, and moisture |
|---|---|---|
| *Very unstable* | | |
| Momentum: ($\zeta < -1.574$) | 5.30 | $\phi_m(\zeta)=0.7k^{2/3}(-\zeta)^{1/3}$ |
| Heat/moist: ($\zeta < -0.465$) | 5.31 | $\phi_h(\zeta)=\phi_w(\zeta)=0.9k^{4/3}(-\zeta)^{-1/3}$ |
| | 5.32 | $V_a=\frac{u_*}{\kappa}\left\{\left[\ln\left(\frac{\zeta_m L}{z_{0m}}\right)-\psi_m(\zeta_m)\right]+1.14\left[(-\zeta)^{1/3}-(-\zeta_m)^{1/3}\right]\psi_m\left(\frac{z_{0m}}{L}\right)\right\}$ |
| *Weakly unstable* | | |
| Momentum: ($-1.574 < \zeta < 0$) | 5.30 | $\phi_m(\zeta)=(1-16\zeta)^{-1/4}$ |
| Heat/moist: ($-0.465 < \zeta < 0$) | 5.31 | $\phi_h(\zeta)=\phi_w(\zeta)=(1-16\zeta)^{-1/2}$ |
| | 5.33 | $V_a=\frac{u_*}{\kappa}\left\{\left[\ln\left(\frac{z_{atm,m}-d}{z_{0m}}\right)-\psi_m(\zeta)\right]+\psi_m\left(\frac{z_{0m}}{L}\right)\right\}$ |
| | 5.36 | $\psi_m(\zeta)=2\ln\left(\frac{1+x}{2}\right)+\ln\left(\frac{1+x^2}{2}\right)-2\tan^{-1}x+\frac{\pi}{2}$ where $x=(1-16\zeta)^{1/4}$ |
| *Weakly stable* | | |
| Mom/heat/moist: ($0 < \zeta < 1$) | 5.30, 5.31 | $\phi_m(\zeta)=\phi_h(\zeta)=\phi_w(\zeta)=1+5\zeta$ |
| | 5.34 | $V_a=\frac{u_*}{\kappa}\left\{\left[\ln\left(\frac{z_{atm,m}-d}{z_{0m}}\right)+5(\zeta)\right]-5\left(\frac{z_{0m}}{L}\right)\right\}$ |
| *Very stable* | | |
| Mom/heat/moist: ($1 < \zeta$) | 5.30, 5.31 | $\phi_m(\zeta)=\phi_h(\zeta)=\phi_w(\zeta)=5+\zeta$ |
| | 5.35 | $V_a=\frac{u_*}{\kappa}\left\{\left[\ln\left(\frac{L}{z_{0m}}\right)+5\right]+[5\ln(\zeta)+\zeta-1]-5\left(\frac{z_{0m}}{L}\right)\right\}$ |

*Note.* In the unstable expressions, $\psi_m$ is the diabatic term in the integrated momentum equation. Also shown is the full form of the integrated momentum equation used to calculate the above-canopy mean wind speed $V_a$.

CLM4.5 has an internal variable (*zetamaxstable*, $\zeta^{max}_{stable}$) that sets a limit on how large $\zeta$ can become. The CLM4.5 default value is 2 (shown as a dashed vertical line in Figure 10), and we will discuss the effect of changes to $\zeta^{max}_{stable}$ on the CLM4.5 output in section 3.7.4.

**Table 4**
*Universal Similarity Functions for Momentum $\phi_m$, Heat $\phi_h$, and Moisture $\phi_w$ Examined in Our Study*

| Universal functions for momentum, heat, and moisture | | Stability range |
|---|---|---|
| *CLM4.5* (Zeng et al., 1998) | | |
| Momentum | $\phi_m(\zeta)=0.7k^{2/3}(-\zeta)^{1/3}$ | $\zeta < -1.574$ |
| | $\phi_m(\zeta)=(1-16\zeta)^{-1/4}$ | $-1.574 \le \zeta < 0$ |
| | $\phi_m(\zeta)=1+5\zeta$ | $0 \le \zeta \le 1$ |
| | $\phi_m(\zeta)=5+\zeta$ | $1 < \zeta$ |
| Heat/moisture | $\phi_h(\zeta)=\phi_w(\zeta)=0.9k^{4/3}(-\zeta)^{-1/3}$ | $\zeta < -0.465$ |
| | $\phi_h(\zeta)=\phi_w(\zeta)=(1-16\zeta)^{-1/2}$ | $-0.465 \le \zeta < 0$ |
| | $\phi_h(\zeta)=\phi_w(\zeta)=1+5\zeta$ | $0 \le \zeta \le 1$ |
| | $\phi_h(\zeta)=\phi_w(\zeta)=5+\zeta$ | $1 < \zeta$ |
| *Högström* (1988) *(based on Businger et al.* (1971)) | | |
| Momentum | $\phi_m(\zeta)=(1-19.3\zeta)^{-1/4}$ | $-2 < \zeta < 0$ |
| | $\phi_m(\zeta)=1+6\zeta$ | $0 < \zeta < 1$ |
| Heat/moisture | $\phi_h(\zeta)=\phi_w(\zeta)=0.95(1-11.6\zeta)^{-1/2}$ | $-2 < \zeta < 0$ |
| | $\phi_h(\zeta)=\phi_w(\zeta)=0.95+7.8\zeta$ | $0 < \zeta < 1$ |
| *Handorf et al.* (1999) | | |
| Momentum | $\phi_m(\zeta)=1+5\zeta$ | $0 < \zeta < 0.6$ |
| | $\phi_m(\zeta)=4$ | $0.6 < \zeta$ |
| Heat/moisture | $\phi_h(\zeta)=\phi_w(\zeta)=1+5\zeta$ | $0 < \zeta < 0.6$ |
| | $\phi_h(\zeta)=\phi_w(\zeta)=4$ | $0.6 < \zeta$ |

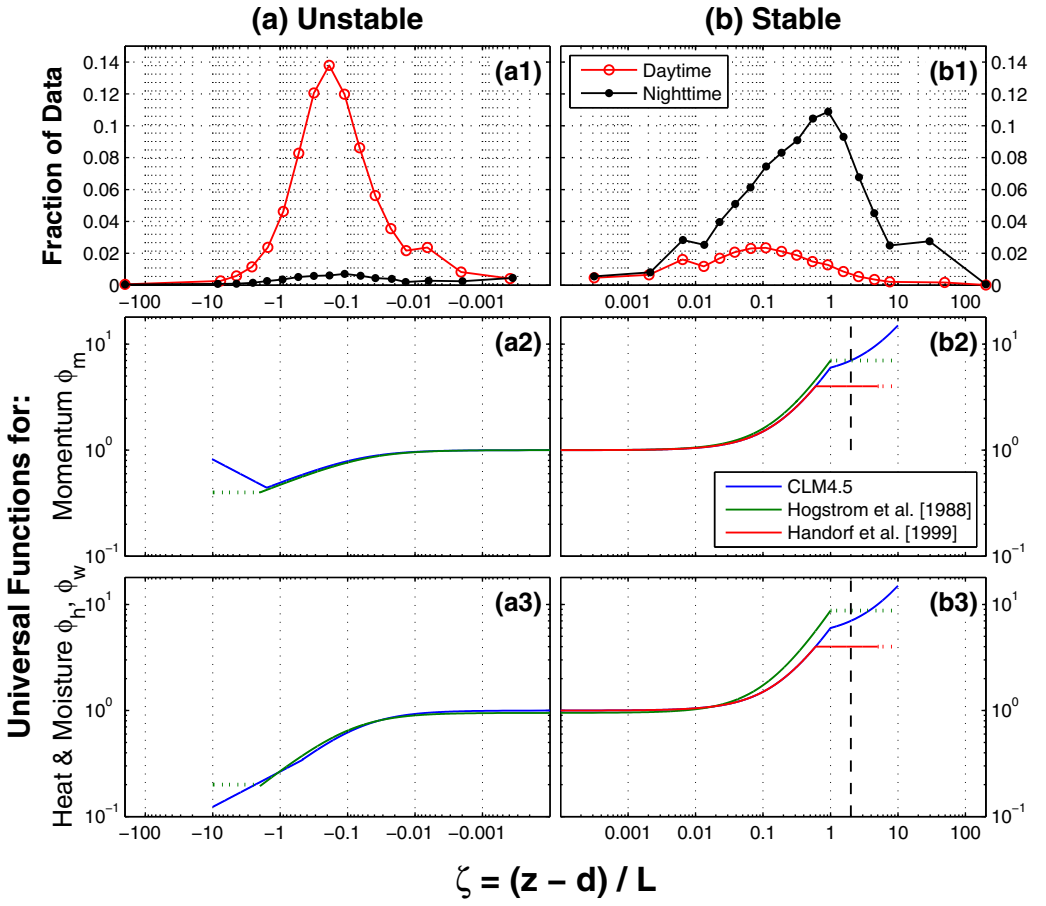


**Figure 10.** The frequency distribution of the dimensionless stability parameter $\zeta=(z-d)/L$ at the US-NR1 site measured at 21.5 m above the ground for (a1) unstable and (b1) stable conditions. These data are from 16 years of tower measurements (1999–2014) between June and September. The results are shown as the fraction of the total points for daytime (incoming PAR $>$ 50 $\mu$mol m$^{-2}$ s$^{-1}$) and nighttime (incoming PAR $<$ 1 $\mu$mol m$^{-2}$ s$^{-1}$) periods, as specified in the legend of Figure 10b1. For the daytime data, 78.7% of the periods are unstable, and for nighttime data, 94.0% of the periods are stable. Below that, the universal similarity functions for (a2, b2) momentum $\phi_m$ and (a3, b3) heat $\phi_h$ and moisture $\phi_w$ are shown as a function of $\zeta$. The relationships shown are from CLM4.5 (i.e., Zeng et al., 1998), Högström (1988) (based on Businger et al. (1971)), and Handorf et al. (1999), as specified in the legend of Figure 10b2. Handorf et al. (1999) is only defined in stable conditions and the $\phi$ values used outside of the defined $\zeta$ range are shown as dotted lines. In Figures 10b2 and 10b3, the vertical dashed line is the default value of *zetamaxstable*, $\zeta^{max}_{stable}=2$. Note that $\phi_h=\phi_w$ for all formulations shown.

### 3.7.2. Stable Conditions in CLM4.5

The value chosen for the CLM4.5 variable *zetamaxstable* $\zeta^{max}_{stable}$ strongly impacts $u_*$ and the stability parameter $\zeta$. For the CLM4.5 A1 configuration, a time series of $\zeta$ shows that $\zeta$ was almost always pegged at $\zeta^{max}_{stable}=2$, which determines the value of the universal function (supporting information Figure S3a). Here it can also be observed that CLM-calculated $u_*$ was smaller than the observed $u_*$ at night, as discussed in section 3.5.1. If $\zeta^{max}_{stable}$ was changed to a value of 100, then $\zeta$ became fixed at 100, and $u_*$ was very small (CLM4.5 D0; supporting information Figure S3b). This is a signature of the positive feedback between $\zeta$ and $u_*$ at night—where a large value of $\zeta$ reduces the turbulence which then leads to even more stable conditions. By using observed $u_*$ we eliminated the possibility of this happening; however with $\zeta^{max}_{stable}$ set to 2 there were still some nights where $\zeta$ was fixed at $\zeta^{max}_{stable}$ (CLM4.5 C0; supporting information Figure S3c). When observed $u_*$ was used and $\zeta^{max}_{stable}$ was set to 100, then the values of $\zeta$ were approximately the same as observed $\zeta$ (CLM4.5 D1; supporting information Figure S3d). The value of $\zeta^{max}_{stable}=100$ was chosen since this is near the upper limit of observed $\zeta$ (Figure 10b1). This example shows the complex interactions between these variables.

### 3.7.3. Sensitivity of CLM4.5 Latent Heat Flux to Observed $u_*$ and Choice of Universal Function

We first examine how using observed $u_*$ (CLM4.5 C0 or D1) affected the default CLM4.5 A1 fluxes and temperatures (from Table 2, the results for C0 and D1 were similar so they will be used interchangeably within our discussion). During the daytime, the difference between CLM4.5 A1 and D1 fluxes (Figures 11a1 and 11b1) and temperatures (Figure 11c1) were small. This is expected because the CLM4.5-derived and observed $u_*$ agree well during the daytime (i.e., Figure 2d).

At night, using observed $u_*$ led to an increase in the magnitude of the net radiation $R_{net}$ as well as the sensible and latent heat fluxes (Figure 11a2). This is expected, since increased $u_*$ should result in increased turbulent mixing and fluxes. Due to these increased fluxes, the nocturnal CLM4.5 canopy and 2 m temperatures increased by ≈1.5°C (Figure 11c2). When the CLM4.5 C0 temperatures are plotted versus $Ri_b$ in Figure 9c1, it can be seen that observed $u_*$ helped limit the continual decrease in CLM temperature in strongly stable

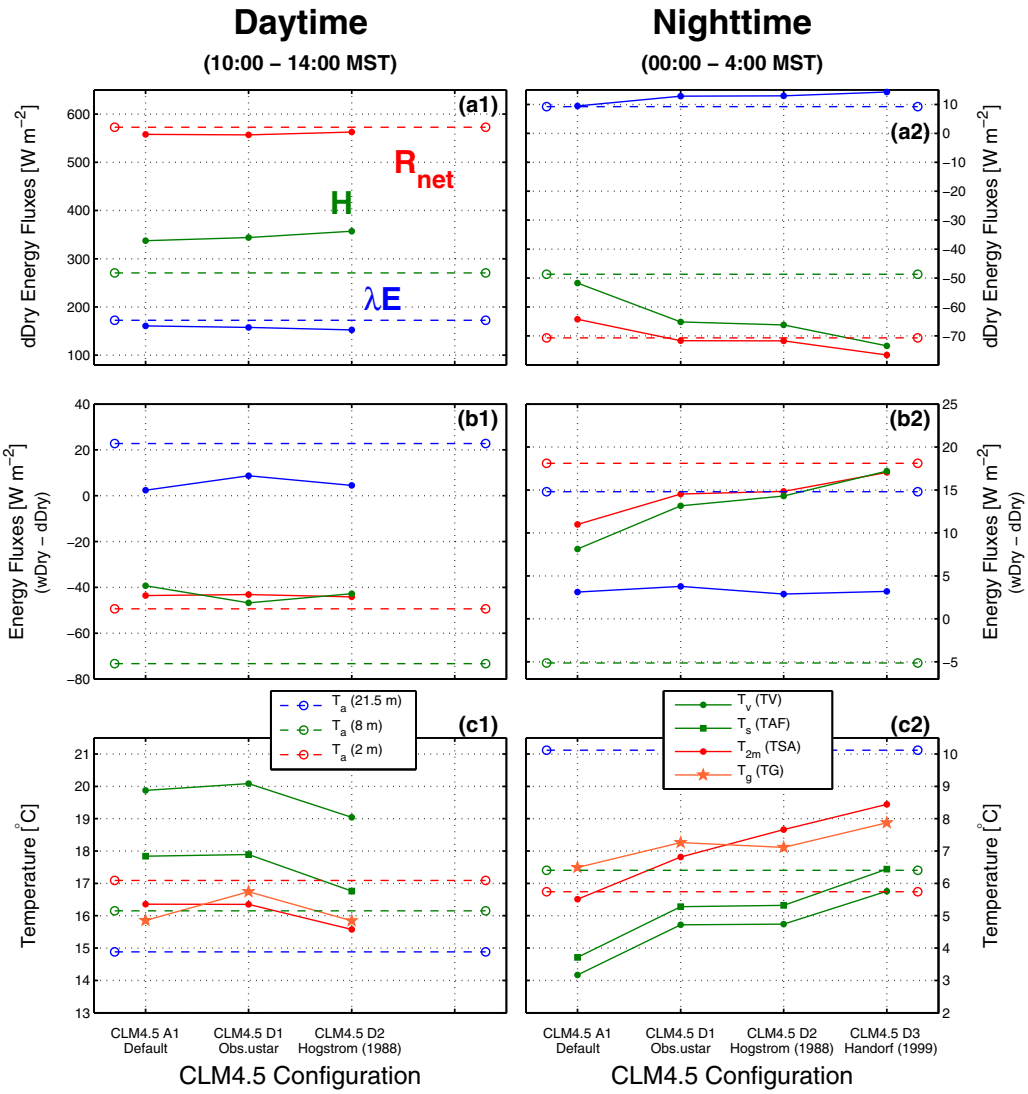


**Figure 11.** The changes in (a1, b1) daytime and (a2, b2) nighttime above-canopy energy fluxes as the CLM4.5 configuration is changed. (top) The mean values for dDry conditions and (middle) the mean differences between wDry and dDry conditions where the variables shown are net radiation $R_{net}$ (red), sensible heat flux $H$ (green), and latent heat flux $\lambda E$ (blue). The solid lines with filled symbols are the CLM4.5 output, while the dashed lines with open circles are the US-NR1 tower observations. (c1, c2) The observed and CLM4.5 temperatures are shown as described in the two legends. Using the alphanumeric code described in Table 1, the CLM4.5 configurations shown from left-to-right are the default A1, which uses the universal function of Zeng et al. (1998); D1 which uses observed $u_*$; D2 which uses the universal function of Högström (1988); and D3 which uses the universal function of Handorf et al. (1999) (only defined in stable conditions).

conditions in a manner similar to the US-NR1 air temperature (Figure 9a1), as discussed in section 3.6. Furthermore, the general shape of the CLM4.5 C0 temperature versus $Ri_b$ curves look similar to the curves from the observations. Using observed $u_*$ in CLM was a first step toward eliminating the nocturnal cold bias in the vegetation temperature and controlling runaway cooling in CLM. This point emphasizes the importance of modeling the basic turbulence variables, such as $u_*$, correctly.

Using the Högström (1988; CLM4.5 D2) and Handorf et al. (1999; CLM4.5 D3) universal functions increased the nocturnal temperatures (especially $T_{2m}$, Figure 11c2) and magnitude of the fluxes even more than CLM5.4 D1. Using observed $u_*$ had a larger effect on the CLM fluxes and temperatures than the choice of universal function.

Though using observed $u_*$ increased the CLM4.5 A1 nocturnal dDry $\lambda E$ value of 9.5 W $m^{-2}$ to over 13 W $m^{-2}$, there was also a corresponding increase in $\lambda E$ during wDry conditions (see the entries for CLM4.5 D1, D2, or D3 in Table 2). Therefore, using observed $u_*$ or a different form of the universal function increased $\lambda E$ in both wet and dry conditions, and only produced a wDry-dDry $\lambda E$ value of around 3 W $m^{-2}$, rather than the 15 W $m^{-2}$ from the US-NR1 observations (Figure 11b2 and Table 2).

#### 3.7.4. Sensitivity of CLM4.5 Latent Heat Flux and Temperature to *zetamaxstable* $\zeta_{stable}^{max}$

Another factor which changes the CLM4.5 fluxes and temperatures is the value of $\zeta_{stable}^{max}$. In Figure 12, we examine the effect of systematically varying $\zeta_{stable}^{max}$ between 0.1 and 100. Of course, the daytime CLM fluxes and temperatures were not affected very much (Figures 12a1, 12b1, and 12c1). For the nighttime periods, as $\zeta_{stable}^{max}$ was increased, the magnitude of the nocturnal dDry fluxes generally became smaller (Figure 12a2) and the CLM4.5 temperatures decreased by ≈2°C (Figure 12c2). Also, there was almost no change in the CLM4.5 fluxes or temperature for $\zeta_{stable}^{max} > 10$. This makes sense if we revisit Figure 10 and realize that only a small percentage of data exist for $\zeta > 10$.

The purpose of $\zeta_{stable}^{max}$ is to limit the CLM4.5 universal functions in strongly stable conditions. This is, for all practical purposes, exactly what the universal function suggested by Handorf et al. (1999) was designed to do—but instead of putting the limit on $\zeta$, the modification was made to the universal functions themselves. As we have shown in the time series of supporting information Figure S3, reasonable values of $\zeta$ can be achieved if $u_*$ is accurate. For this reason, it seems more logical to eliminate the use of $\zeta_{stable}^{max}$ in CLM, and instead use a universal function that becomes a constant in the strongly stable regime, such as that proposed by Handorf et al. (1999).

The other question related to both $\zeta_{stable}^{max}$ and/or a revised universal function is which value of $\zeta$ to use for the cutoff value. It would be logical to have this occur where there is a change in the flow characteristics. In terms of bulk Richardson number, the transition from fully turbulent to stable flow has traditionally been thought to occur at $Ri_b \approx 0.25$. At the US-NR1 site, Burns et al. (2011) found that, for $0.01 < Ri_b < 0.5$, there was a nearly linear relationship between $Ri_b$ and $\zeta$, and for $Ri_b > 0.5$, $\zeta$ became nearly constant at $\zeta \approx 1$. This suggests that (for US-NR1) the universal function should become a constant at $\zeta \approx 1$. This cutoff value agrees well with the universal function of Högström (1988), which, in stable conditions, is only defined for $\zeta < 1$ (Figures 10b2 and 10b3 and Table 4). Handorf et al. (1999) chose a cutoff value of $\zeta = 0.6$ for the stable boundary layer over an Antarctic ice shelf. One would expect this cutoff value to be landscape dependent and a possible range of values would best be determined by comparing results from many sites.

The variation of $\zeta_{stable}^{max}$ shown in Figure 12 is equivalent to changing the $\zeta$ cutoff value for a universal function. Here we can get some idea of the sensitivity of the CLM fluxes and temperature to changing this cutoff value. When the cutoff value was changed from the default value of 2 to 1, the following can be observed: there was a small effect on $\lambda E$, dDry $H$ decreased on the order of 10–15%, and the CLM temperatures increased by ≈0.5°C (Figure 12). Though a more focused study may be needed, our initial results suggest that eliminating $\zeta_{stable}^{max}$ from CLM and using the universal function of Högström (1988), with a constant universal functions for $\zeta > 1$, should produce reasonable CLM results.

### 3.8. Subcanopy Turbulent Exchange in CLM4.5

For forested locations, CLM4.5 includes an additional resistance that represents the turbulent exchange of heat and moisture between the ground surface and the overlying canopy airspace. This turbulent energy

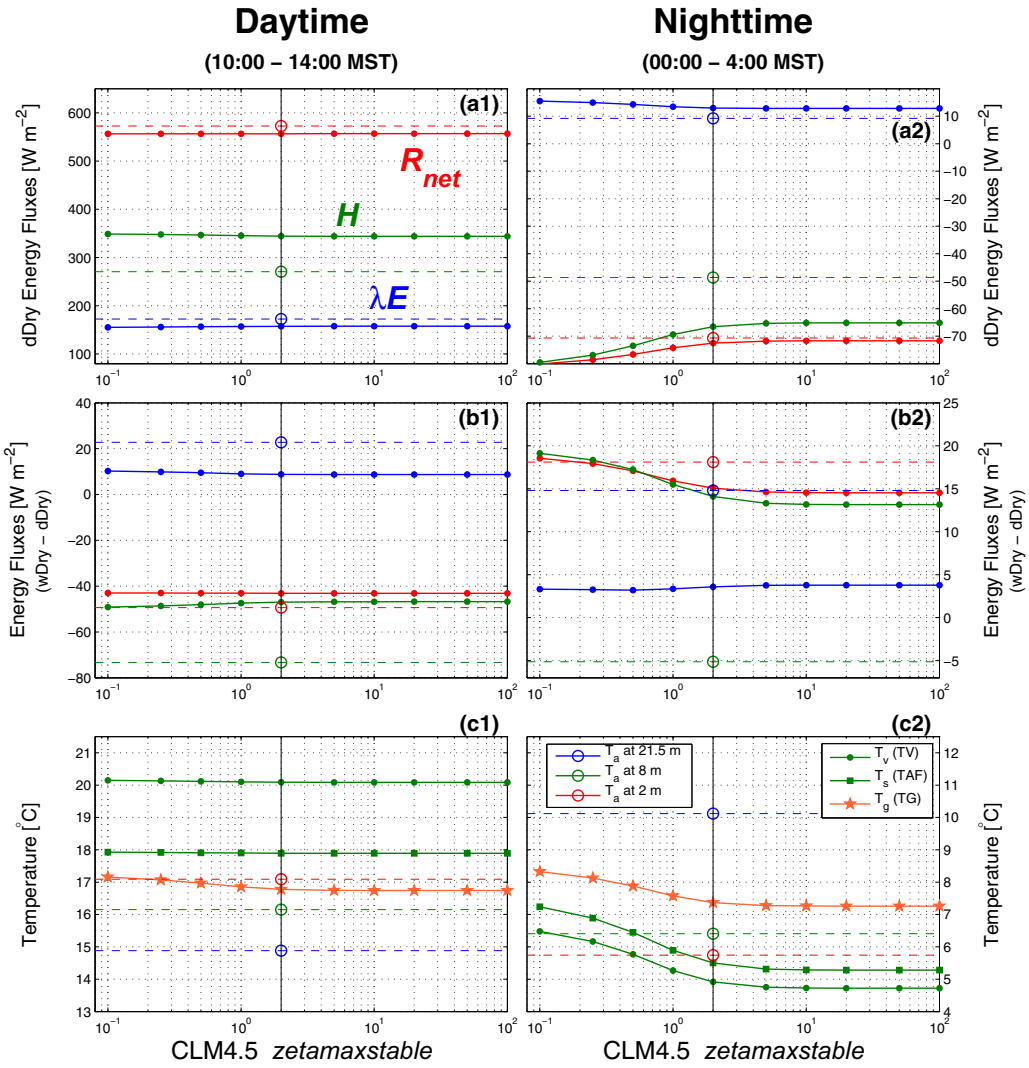


**Figure 12.** (a1, b1) Daytime and (a2, b2) nighttime energy fluxes versus the CLM4.5 variable *zetamaxstable* $\zeta^{max}_{stable}$ as it varies from 0.1 to 100. (top) The mean values for dDry conditions and (middle) the mean differences between wDry and dDry conditions where the variables shown are net radiation $R_{net}$ (red), sensible heat flux $H$ (green), and latent heat flux $\lambda E$ (blue). The solid lines with filled symbols are the CLM4.5 output, while the horizontal dashed lines are the US-NR1 tower observations with open circles (and vertical black line) placed at the CLM4.5 default value of $\zeta^{max}_{stable}=2$. (c1, c2) The US-NR1 observed air temperature $T_a$ and the effect of varying $\zeta^{max}_{stable}$ on CLM canopy surface $T_v$, canopy air $T_s$ and ground $T_g$ temperatures are shown (see legends). The CLM results use the CLM4.5 D1 configuration (Table 1), with $\zeta^{max}_{stable}$ being varied.

exchange is controlled by the aerodynamic resistances for heat $r'_{ah}$ and water vapor $r'_{aw}$, which are assumed to be equivalent, and follow,

$$r'_{ah}=r'_{aw}=\frac{1}{C_s U_{av}}, \tag{5}$$

where $U_{av}$ is the magnitude of the wind velocity on the vegetation and $C_s$ is the turbulent transfer coefficient between the underlying soil and the canopy air. Following Dickinson et al. (1993), $U_{av}$ is roughly estimated based on the above-canopy friction velocity (i.e., $U_{av}=u_*$). Because there are wind speed and turbulence measurements within the subcanopy at US-NR1, we will test/validate the $U_{av}=u_*$ relationship at the US-NR1 site in section 3.8.3.

Subcanopy exchange is known to depend on the canopy density profile within a forest (Zeng et al., 2005). In CLM4.5, $C_s$ is calculated from a linear combination of bare-soil $C_{s,bare}$ and dense canopy $C_{s,dense}$ turbulent transfer coefficients,

$$C_s = C_{s,bare}W + C_{s,dense}(1-W), \tag{6}$$

where $W$ is an exponential function of the leaf and stem-area index. For the US-NR1 site with LAI ≈4, $W$ is around 0.018 and $C_{s,dense}$ is the dominant contributor to $C_s$.

Sakaguchi and Zeng (2009) proposed that $C_{s,dense}$ should depend on the local stability beneath the canopy. This accounts for situations where a dense overstory can lead to a stable understory during the daytime and an unstable understory at night. In extreme cases, such a situation can produce thermotopographic flows within the subcanopy (e.g., Froelich & Schmid, 2006). Sakaguchi and Zeng (2009) assumed that $C_{s,dense}$ =0.004 was appropriate for locally unstable conditions in the subcanopy. To account for locally stable conditions (i.e., a canopy air temperature $T_s$ warmer than the ground $T_g$), Sakaguchi and Zeng (2009) decreased the default $C_{s,dense}$ value of 0.004 following,

$$C_{s,dense} = \begin{cases} 0.004 & T_s - T_g \le 0 \ \text{(locally unstable)}, \\ \dfrac{0.004}{1+\gamma \min(S,10)} & T_s - T_g > 0 \ \text{(locally stable)}, \end{cases} \tag{7}$$

where $\gamma$ is an empirical constant (chosen to be 0.5 by Sakaguchi and Zeng (2009)). $S$ is a stability parameter with a form similar to $\mathrm{Ri_b}$, calculated by

$$S = \frac{gh(T_s - T_g)}{T_s u_*^2}, \tag{8}$$

where $h$ is the canopy height and $u_*$ is evaluated above the canopy (but also represents an average wind speed within the subcanopy airspace, as discussed in section 3.8.3). The upper value of 0.004 for $C_{s,dense}$ was originally proposed by Dickinson et al. (1993), and it is not entirely clear how that specific value was determined. As discussed by Zeng et al. (2005), values for $C_{s,dense}$ on the order of ≈0.04 have been proposed by others (e.g., Bonan, 1996; Lo Seen et al., 1997). Next, we examine the sensitivity of CLM4.5 output to variations in $C_{s,dense}$ and discuss the appropriateness of the Sakaguchi and Zeng (2009) correction (hereafter, labeled the "S-Z" correction).

#### 3.8.1. Sensitivity of CLM4.5 Latent Heat Flux and Temperature to the Subcanopy Turbulent Transfer Coefficient $C_{s,dense}$

During the daytime, as $C_{s,dense}$ was increased from 0.001 to 40 (the CLM4.5 default value is 0.004), changes to $R_{\mathrm{net}}$ (Figures 13a1 and 13b1) and $T_v$ and $T_s$ temperatures (Figure 13c1) were generally small. However, as $C_{s,dense}$ was increased from 0.004 to ≈0.1, the ground temperature $T_g$ increased and became very close to the canopy air temperature $T_s$. This implies that larger values of $C_{s,dense}$ increased the turbulent heat exchange between the atmosphere and the ground, warming the soil. During the daytime we have shown that $T_a$ within the US-NR1 subcanopy was fairly well mixed, creating a nearly constant $T_a$ profile. This implies that increasing $C_{s,dense}$ to the point where $T_g \approx T_s$ might be realistic.

The effect of increased $C_{s,dense}$ on the CLM midday fluxes is shown in Figure 13a1, where dDry sensible heat flux increased at the expense of the latent heat flux. As $C_{s,dense}$ was increased, wDry-dDry $\lambda E$ increased from just-above zero for $C_{s,dense}$=0.001, to a value of around 70 W m$^{-2}$ at $C_{s,dense} \approx 0.4$ (Figure 13b1). This was much larger than the US-NR1 wDry-dDry $\lambda E$ value of ≈25 W m$^{-2}$ (shown as a blue dashed line in Figure 13b1). This suggests that during a wDry day water was available to evaporate in CLM4.5, but $C_{s,dense}$ set at 0.004 limited this evaporation.

At night, as $C_{s,dense}$ was increased, the wDry-dDry $\lambda E$ difference increased dramatically to ≈16 W m$^{-2}$ (for $C_{s,dense} > 4$) which was just-above the observed wDry-dDry $\lambda E$ value (Figure 13b2). While we do not necessarily advocate that $C_{s,dense}$ should be increased from 0.004 to 4 (a factor of 1,000), this example shows that changes to $C_{s,dense}$ can significantly impact nocturnal $\lambda E$ in wet conditions.

For increased $C_{s,dense}$, the CLM4.5 nocturnal air and canopy temperatures all increased, while $T_g$ decreased (Figure 13c2), suggesting that heat was extracted from the soil and added to the atmosphere. (As discussed previously, the CLM nocturnal temperatures seemed more reasonable using observed $u_*$, so in Figure 13

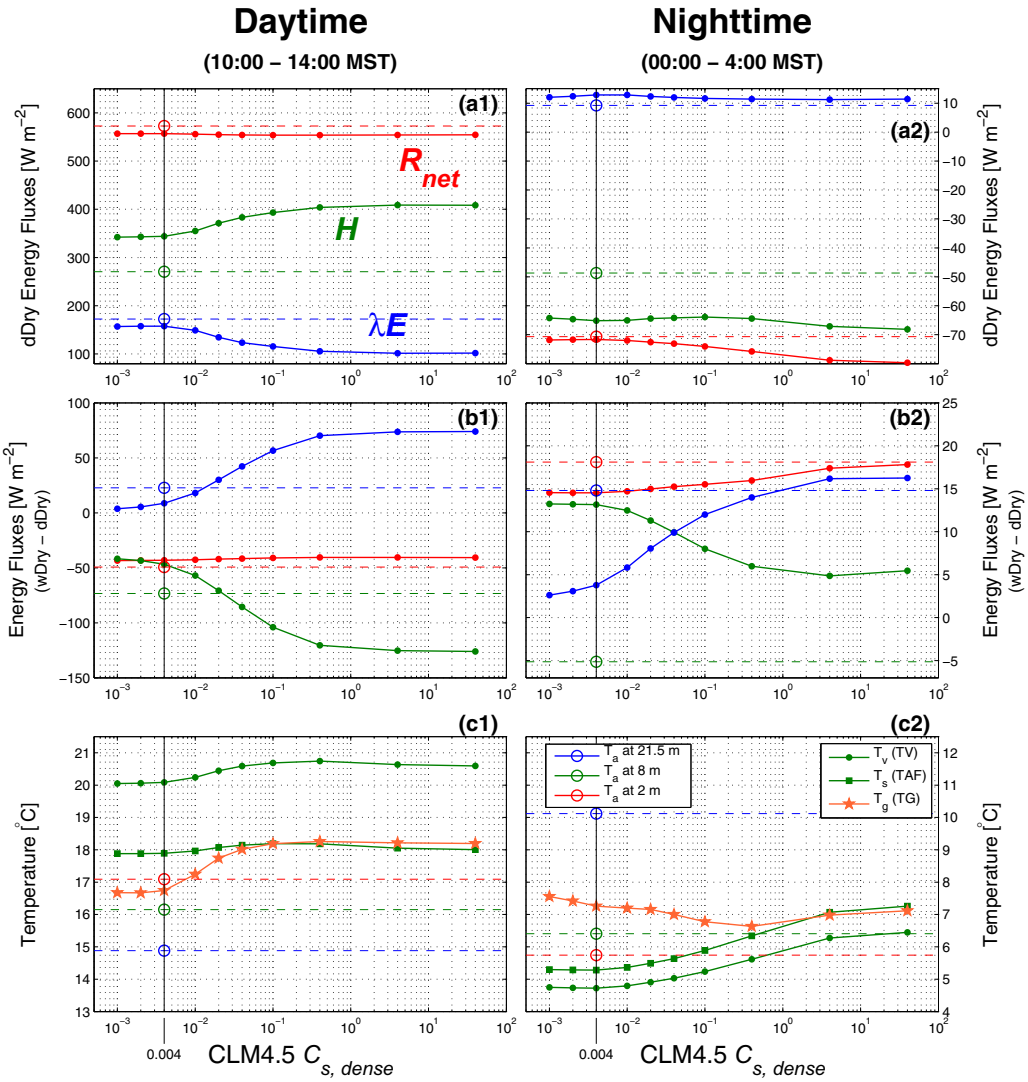


**Figure 13.** Similar to Figure 12, except that the CLM4.5 dense canopy turbulent transfer coefficient $C_{s,dense}$ is varied from 0.001 to 40 (the CLM4.5 default value is $C_{s,dense}$=0.004). The CLM results use the CLM4.5 F2 configuration (see Table 1 for details), with $C_{s,dense}$ being varied.

observed $u_*$ was used.) If we look at the US-NR1 vertical $T_a$ profile in Figure 8b, the coldest air was located near the ground which implies that the ground surface was the coldest location, not the canopy as suggested by CLM. From Figure 13c2, it is clear that $C_{s,dense}$ affects the relationship between $T_g$ and $T_s$, and, at $C_{s,dense} \approx 0.4$, $T_s$ approaches $T_g$.

In order to better understand how $C_{s,dense}$ affected the CLM latent heat flux, the components of $\lambda E$ are plotted in Figure 14 as $C_{s,dense}$ was varied. In dDry midday conditions, there was a decrease in $\lambda E$ as $C_{s,dense}$ was increased due to changes in $H$ (as discussed above, and shown in Figure 13a1). The ground evaporation term increased slightly as $C_{s,dense}$ increased from 0.001 to 0.01, and then leveled off for $C_{s,dense} > 0.01$ (Figure 14a1). However, for midday wDry-dDry, it was the ground evaporation term that contributed most to $\lambda E$, and the magnitude of the ground evaporation was highly dependent on the value of $C_{s,dense}$ (Figure 14b1). At night, the transpiration and ground evaporation in dDry conditions were both at around 5 W m$^{-2}$ with only a weak dependence on $C_{s,dense}$ (Figure 14a2). In wet conditions, the nocturnal transpiration decreased (which is why wDry-dDry for transpiration is negative in Figure 14b2), and ground evaporation increased. Similar to the daytime, the magnitude of nocturnal ground evaporation was very sensitive to the choice of $C_{s,dense}$.

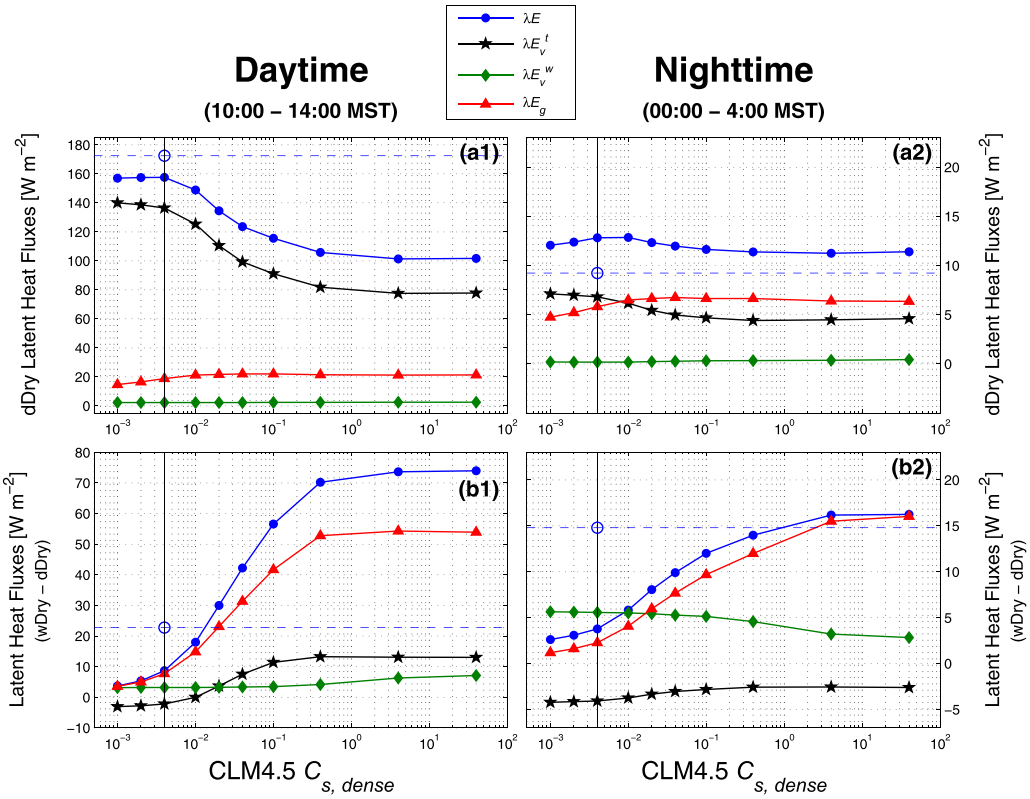


**Figure 14.** (a1, b1) Daytime and (a2, b2) nighttime latent heat flux $\lambda E$ components versus the CLM4.5 dense canopy turbulent transfer coefficient $C_{s,dense}$ as it is varied from 0.001 to 40. (top) The mean values for dDry conditions and (bottom) the mean differences between wDry and dDry conditions where the $\lambda E$ components (described in the legend) are: total latent heat flux $\lambda E$; canopy transpiration $\lambda E_v^t$; canopy evaporation $\lambda E_v^w$; and ground evaporation $\lambda E_g$. The solid lines with filled symbols are the CLM4.5 output, while the horizontal dashed lines are the US-NR1 observed $\lambda E$ with open circles (and vertical black line) placed at the CLM4.5 default value of $C_{s,dense} = 0.004$. The CLM results use the CLM4.5 F2 configuration (Table 1), with $C_{s,dense}$ being varied.

For our study, we are conservative, and examine the effect of increasing $C_{s,dense}$ from the default value of 0.004 to 0.01 (i.e., CLM4.5 F0, F1, and F2 in Table 1). The value of 0.01 was chosen because it produced a midday wDry-dDry $\lambda E$ value that was close to the observations (Figure 13b1); however, the nighttime data suggest that $C_{s,dense}$ could be increased even further. As discussed by others (e.g., Sakaguchi & Zeng, 2009; Zeng et al., 2005), the real issue is that $C_{s,dense}$ cannot be assumed a constant and should depend on the conditions at the site. For simplicity and consistency, we have left $C_{s,dense}$ as a constant in our study, but the validity of using a constant $C_{s,dense}$ needs further examination.

### 3.8.2. Correction of Sakaguchi and Zeng (2009)

For US-NR1, the S-Z correction (equation (7)) does not achieve satisfactory results for reasons we explain herein. First, the subcanopy air (and thus $T_a$) was, on average, well mixed during the daytime, and the ground surface was directly cooled by longwave radiation at night (Figure 8). The S-Z correction was designed for situations where a drastic temperature difference between the canopy and ground exists, which US-NR1 does not have. Second, the S-Z correction did not work well at US-NR1 at night due to the unreasonably cold canopy bias (using CLM4.5 A1) which created very unstable (and unrealistic) conditions in the subcanopy (Figure 9). However, even after the CLM temperatures were made more reasonable (e.g., by using observed $u_*$), the S-Z correction still seems problematic because it was very small in the most stable conditions (Figure 9c2).

We also need to consider the magnitude and direction of the S-Z correction. As mentioned by Sakaguchi and Zeng (2009), the S-Z correction that they proposed is "conservative." On average, the S-Z correction reduced $C_{s,dense}$ by about a factor 0.7 at night (red line in Figure 9c2) and 0.6 during the daytime (red line in supporting information Figure S4c2). This means that, in general,

the S-Z correction reduced $C_{s,dense}$ from 0.004 to somewhere between 0.0016 and 0.0028. In Figure 13, one can observe that such changes to $C_{s,dense}$ would lead to very small changes to the CLM fluxes and/or temperatures. Furthermore, as shown in Figure 13 (and discussed in the previous section), it is by increasing $C_{s,dense}$ that significant changes to CLM output occurred. While the value of 0.004 might be appropriate for certain forest types, it does not appear to work well at the US-NR1 coniferous forest site. In short, it should be considered whether 0.004 is an appropriate upper value of $C_{s,dense}$ (or not). For more discussion, see section 4.1.

#### 3.8.3. Relationship Between $u_*$ and Subcanopy Wind

As part of the subcanopy turbulent parameterization, it is assumed that the wind velocity on the vegetation $U_{av}$ is linearly related to above-canopy friction velocity, i.e., $U_{av}=u_*$. Surprisingly, we could not find any study that checked or confirmed this relationship. This expression was first suggested by Dickinson et al. (1993) and then adopted into CLM4.5. At the US-NR1 site, we used two sonic anemometers located in the mid and lower portion of the canopy to show that the subcanopy mean wind speed $U$ has very little connection to above-canopy $u_*$ (supporting information Figure S5). If we make an assumption that subcanopy $U \approx U_{av}$, then using $U_{av}=u_*$ will lead to an overestimate of $U_{av}$ by about a factor of 2 in high above-canopy winds, and an underestimation of $U_{av}$ in low winds. Somewhere in the upper canopy it is possible that $U_{av}=u_*$ is appropriate. This is an example of the complexity of flow within a forest canopy and one of the challenges of using a simple big-leaf type of model to represent this complexity.

Air motions in the subcanopy are largely controlled by the canopy-generated coherent structures just-above canopy top (Raupach et al., 1996) and associated pressure fronts (Shaw & Zhang, 1992). Or, in complex terrain, by the local topography (Burns et al., 2011). For a big-leaf model, the meaning of $U_{av}$ is difficult to define because the wind velocity varies from some finite value in the forest gaps to zero at the leaf and branch surfaces. This subject goes beyond the scope of the current paper but is a possible future topic of study.

## 4. Final Comments and Speculations

### 4.1. Contrasting the Effect of Decreasing $f_{wet}^{max}$ Versus Increasing $C_{s,dense}$ on CLM Latent Heat Flux

We found that increased midday wDry-dDry $\lambda E$ can be achieved by either decreasing $f_{wet}^{max}$ from 1 to 0.02 (Figure 5b1) or by increasing $C_{s,dense}$ from 0.004 to 0.01 (Figure 13b1). Modified $f_{wet}^{max}$ increased CLM wDry $\lambda E$ by modifying the timing and magnitude of the canopy evaporation term, whereas modified $C_{s,dense}$ increased the ground evaporation term. In order to better understand any nonlinear or confounding effects of the S-Z correction or using observed $u_*$, we have plotted the $\lambda E$ components for CLM4.5 B0, B1, and B2 in supporting information Figure S6, and those for CLM4.5 F0, F1, and F2 in supporting information Figure S7. As discussed in section 3.4, the changes to $f_{wet}^{max}$ nicely reproduced two aspects of the observations: (1) the timing and magnitude of the increase of midday $\lambda E$ on a wDry day and (2) the shape of $\lambda E$ on the afternoon of a wet day (relative to a dDry day). These features remain regardless of the S-Z correction (supporting information Figure S6b) or the use of observed $u_*$ (supporting information Figure S6c). For increased $C_{s,dense}$, the increase of midday wDry-dDry $\lambda E$ occurred most strongly when observed $u_*$ was used (supporting information Figure S7c). In addition, for CLM4.5 F0, F1, and F2, $\lambda E$ on the afternoons of dWet and wWet days does not look very much like the observations (i.e., Figure 3b).

If we only consider a wDry day (Figure 6c) we can see that observed $\lambda E$ between 0 and 4 MST was about 10 W $m^{-2}$ larger than the dDry value, whereas between 19 and 24 MST $\lambda E$ approached the dDry value. This means that the contribution of evaporation to the enhancement of $\lambda E$, on average, lasts about 18 h following a wet day (Burns et al., 2015). This implies that CLM canopy and ground evaporation terms should be higher on a wDry early morning and smaller on a wDry evening. As shown in Figure 6c, the canopy evaporation term behaved that way for the CLM4.5 B1 and B2 configurations. In contrast, for ground evaporation, the magnitude of early morning and evening $\lambda E_g$ were almost the same. This, coupled with the fairly symmetric shape of the ground evaporation around noon, suggest that the ground evaporation term in CLM is unrealistic during a wDry day.

As discussed in section 3.8.1, CLM ground evaporation is sensitive to the value of $C_{s,dense}$. These analyses suggest that the parameterization of subcanopy turbulent transfer (i.e., $C_{s,dense}$) and the related S-Z

correction could be revisited and/or improved in CLM. This would best be achieved by looking at different forest types in a variety of terrain (flat, simple slopes, and mountainous) and over a wide range of stabilities, similar to what was done by Zeng et al. (2005). Such a study would determine the site characteristics and atmospheric conditions that most affect $C_{s,dense}$, as well as whether using a constant value for $C_{s,dense}$ is appropriate.

To examine the effect of changing $C_{s,dense}$ and $f_{wet}^{max}$ at the same time, we included the CLM4.5 G1 configuration in our study (Tables 1 and 2). In supporting information Figures S8-S10, we have repeated Figures 2, 7, and 8 using the CLM4.5 G1 configuration. From supporting information Figure S9, it is apparent that CLM $\lambda E$ can be increased in strongly stable conditions. Supporting information Figure S10 shows how the CLM nocturnal temperatures increase by around 1.5°C with the G1 settings.

### 4.2. Cumulative Effects of Revised CLM4.5 Parameters

In our study, we have examined 14 different CLM4.5 configurations (Table 1) with the statistics for each configuration shown in Table 2. Since we have focused on the diel cycle, an obvious question is how different are the long term, cumulative fluxes for these 14 possible changes to CLM. Such knowledge, for example, has implications related to the total amount of water transported from an ecosystem to the atmosphere over a season (e.g., Knowles et al., 2015b). The far-right-hand column of Table 2 shows (in bold font for $\lambda E$) the percent difference between the CLM4.5 cumulative water loss relative to the US-NR1 observed water loss over the 2010 warm season (for US-NR1, this was 735.5 MJ $m^{-2}$, or around 298 mm of water lost for every square meter of the forest). CLM4.5 A1 with LAI = 4 had a 2010 warm-season cumulative $\lambda E$ value of 719.5 MJ $m^{-2}$, which was 2.2% smaller than the US-NR1 observations. For all 14 combinations, the difference from US-NR1 ranged from 4% lower then US-NR1 to around 4% larger. For the configuration with all variables modified (CLM4.5 G1), cumulative $\lambda E$ was 0.9% larger than the US-NR1 observations. Though our focus is on $\lambda E$, we note that changes to cumulative CLM $H$ were on the order of 25% different from US-NR1 and more sensitive to the choice of CLM configuration (Table 2).

### 4.3. Asymmetry in the Diel Pattern of Latent Heat Flux

Because we are interested in the diel cycle, a close look at Figure 2 reveals that, for dDry conditions, observed $R_{net,}$ $H$, and $\lambda E$ all peaked just before noon. Burns et al. (2015) showed that the primary reason the observed fluxes peaked prior to noon was due to the common occurrence of afternoon clouds at the US-NR1 site (generated by the dynamics of the mountain-plain circulation). If only days with clear skies were examined, then these variables peak close to noon. While CLM4.5 does a fairly good job on the timing of the peak for $R_{net}$ and $H$, CLM $\lambda E$ peaks near noon, rather than before noon (Figure 2c). In Figure 15, we have separated the dDry diel cycle into periods with any sky condition (left-side figures) and those with clear skies (right-side figures). In Figure 15, top, we have included the vapor pressure deficit VPD measured at the site along with $\lambda E$. Here we can see the the peaks in CLM $\lambda E$ and VPD were both at around noon in all-sky conditions (Figure 15a1) and shifted toward around 14:00 MST for clear skies (Figure 15b1). In contrast, the timing of the peak in observed $\lambda E$ shifted from around 11:00 MST in all-sky conditions to just before noon with clear skies. It seems that the peak in CLM $\lambda E$ follows observed VPD, while observed $\lambda E$ does not. There are several possible explanations for this mismatch in the timing of the CLM $\lambda E$ peak: observed $\lambda E$ is affected by larger-scale atmospheric processes which are unknown to CLM, such as entrainment of dry air at the top of the boundary layer (Betts, 2009; Gentine et al., 2011; van Heerwaarden et al., 2010) or large eddies that impact the near-surface turbulence (Patton et al., 2016); or, it could be related to improper modeling of the US-NR1 tree hydrodynamics (e.g., Matheny et al., 2014).

If we compare the timing of the temperatures peaks in all-sky (Figure 15a2) versus clear-sky (Figure 15b2) conditions, we can make the following conclusion: the peak in above-canopy air temperature during clear-sky conditions was later (at ≈15:00 MST), the peak in soil temperature (at −5 cm) was relatively unaffected by the sky conditions, the peak in observed 2 m air temperature was shifted to a later time, somewhere between the peaks in $T_{soil}$ and above-canopy $T_a$, and the timing of VPD peaks followed $T_a$. The shift in timing of the above-canopy $T_a$ is presumably due to the biomass of the forest accumulating heat when the incoming shortwave irradiance is highest (i.e., on clear-sky days), and then slowly releasing it back to the atmosphere. The CLM4.5 canopy air temperature $T_s$ generally followed the pattern of observed $T_a$. However,

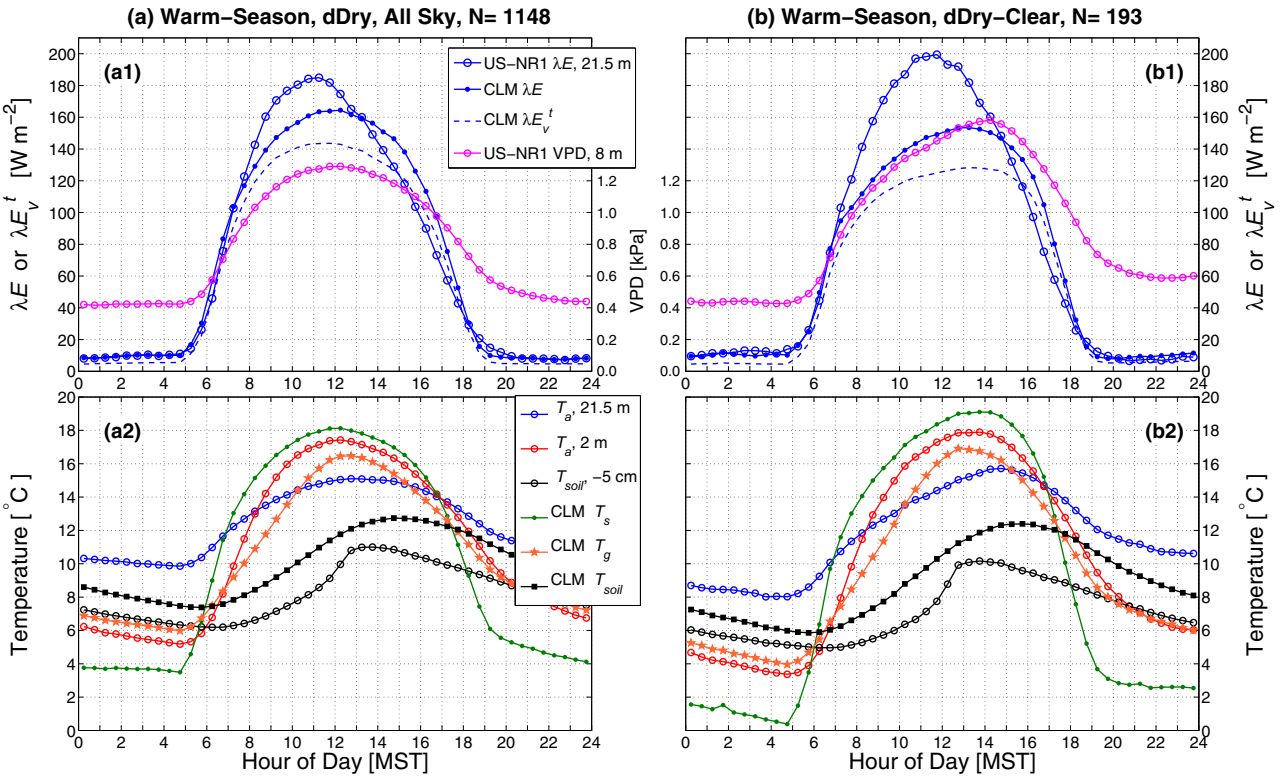


**Figure 15.** The dDry warm-season composite diel cycle of (a1, b1) the US-NR1 above-canopy latent heat flux $\lambda E$ and vapor pressure deficit VPD (middle axis) with CLM4.5 $\lambda E$ and canopy transpiration $\lambda E_v^t$, and (a2, b2) US-NR1 observed 21.5 and 2 m air temperature $T_a$ and soil temperature $T_{soil}$ at −5 cm depth, along with CLM4.5 canopy air temperature $T_s$, ground temperature $T_g$, and $T_{soil}$ at −6.5 cm depth. Figures 15a1 and 15a2 are for all dDry conditions while Figures 15b1 and 15b2 are dDry days with clear skies; the number of days ($N$) that satisfy each condition are listed above the top figure. The legends in Figure 15a also apply to Figure 15b.

observed $T_{soil}$ peaked at around 13:00 MST, while CLM $T_{soil}$ peaked at around 15:00 MST, suggesting that the CLM soil thermal properties or amount of shading is incorrect. The heat capacity of vegetation biomass and soil is an important consideration to properly balance the surface energy budget (e.g., Lindroth et al., 2010; Leuning et al., 2012).

### 4.4. The Effect of Sloped Terrain on Latent Heat Flux

CLM4.5 could not simulate the enhanced latent heat flux at night during wet conditions at US-NR1. Our hypothesis is that enhanced nocturnal $\lambda E$ was due to two phenomena: (1) the presence of liquid water, providing a source for evaporation and (2) the ever-present slope/drainage flow supplying additional energy to drive the evaporation.

To explore this possibility, we examined data from the Howland Forest AmeriFlux site (US-Ho1). Howland Forest was chosen because it has a forest similar to that of US-NR1, but with flatter, rolling terrain. The results from US-Ho1 showed that while US-Ho1 has enhanced $\lambda E$ at midday on a wDry day, it did not show increased $\lambda E$ on wet nights (supporting information Figure S11). US-Ho1 nocturnal $\lambda E$ was very small for both wet and dry conditions which was similar to CLM nocturnal $\lambda E$ from US-NR1. Though our discussion here is focused on the possible effects of slope flow on $\lambda E$, we cannot rule out the possibility that the larger LAI at US-Ho1 (US-Ho1 LAI ≈ 5.5 versus US-NR1 LAI ≈ 4) also contributes to a smaller US-Ho1 nocturnal $\lambda E$. One way to better explore this parameter space would be to look at many sites with a wide range of LAI values and topographic slopes.

Are there features we can examine to highlight something unique about sloped terrain? It is known that the relationship between $u_*$ and wind speed depends on the underlying surface type and roughness (e.g., Blanken et al., 2003). We explored this relationship for both US-NR1 and US-

Ho1 and found that US-Ho1 (and CLM for that matter) exhibited a nearly monotonic increase in $u_*$ with increasing wind speed during midday and at night (supporting information Figure S12). At US-NR1, however, nocturnal $u_*$ was enhanced for low winds (shown as a "hump" at $U \approx 2$ m s$^{-1}$ in supporting information Figure S12b2). This, we suspect, is a signature of the drainage flow. At night, CLM-calculated $u_*$ shows a monotonic increase with wind speed, as well as the low bias discussed in section 3.5.1 (Figure S12b2). MOST should not be expected to calculate an accurate value of $u_*$ during light winds in sloping terrain.

Since we used observed $u_*$ as an input into CLM, should that account for the turbulence in the drainage flow? One might expect this, however the turbulence measured above the canopy is not necessarily the same as what is happening near the ground. This is especially true in a slope flow which can be seen in supporting information Figure S5c, where the lowest values of above-canopy $u_*$ ($<$0.25 m s$^{-1}$) led to an increase in the 2.5 m horizontal wind speed $U$. This provides evidence that what is happening above the canopy is not representative of the ground surface, where drainage winds are likely stronger and promoting surface evaporation. Despite several previous studies related to the horizontal advection at US-NR1 (e.g., Sun et al., 2007; Yi et al., 2005, 2008) how the drainage flow affects the above-canopy fluxes and how representative the above-canopy flux is of the actual flux at the ground surface remains poorly understood.

## 5. Summary and Conclusions

Over a decade of 30 min turbulent flux measurements from just-above a high-elevation subalpine forest at AmeriFlux site US-NR1 were analyzed with a focus on how precipitation perturbed the fluxes on a diel time scale and how well a land-surface model represented these changes. The analysis methodology followed that of Burns et al. (2015) where each day was classified as either wet or dry. From the tower measurements, two results related to the effect of warm-season precipitation on the latent $\lambda E$ and sensible $H$ heat flux were highlighted: (i) for a day following an above-average wet day, midday latent heat flux was enhanced by around 40 W m$^{-2}$ relative to dry conditions, with a concomitant reduction in sensible heat flux and (ii) in wet conditions, nocturnal latent heat flux increased by about 15 W m$^{-2}$ relative to latent heat flux in dry conditions (Figure 1).

We used these two features of the measured turbulent fluxes as a framework for testing the Community Land Model (CLM), version 4.5 (Oleson et al., 2013). Investigation into what controlled CLM latent heat flux necessitated examination of several other aspects of CLM4.5: the maximum permissible amount of water captured by the vegetation, the assumptions and parameterization of the subcanopy turbulent transport, and the MOST universal similarity functions. An additional tool used to evaluate CLM was from a vertical air temperature profile (11 levels), which revealed that CLM nocturnal temperatures had a cold bias of around 2–4°C and evidence of runaway cooling (Figures 8 and 9). Conclusions from our comparison between the US-NR1 tower observations and CLM4.5 modeled fluxes and temperature are the following:

1. Using the default CLM configuration, midday latent heat flux did not increase for a dry day following an above-average wet day as seen in the observations and described in (i) above (thus, CLM sensible heat flux did not decrease as in the observations). By decreasing the *maximum leaf wetted fraction* $f_{wet}^{max}$ from a default value of 1 to 0.02 the timing and magnitude of the canopy evaporation in CLM was modified in such a way that CLM was able to mimic the observations described in (i). It also resulted in $\lambda E$ on the afternoon of wet days that looked similar to observed $\lambda E$.
2. CLM ground evaporation was found to (primarily) be controlled by the subcanopy turbulent transfer coefficient $C_{s,dense}$. When $C_{s,dense}$ was increased from a default value of 0.004 to 0.01, CLM $\lambda E$ behaved as observed $\lambda E$ described in (i) above (Figure 13b1). A comparison of the effect of increasing $C_{s,dense}$ or decreasing $f_{wet}^{max}$ on overall $\lambda E$ suggested that the changes to $f_{wet}^{max}$ were closer to the observed $\lambda E$ (Figure 6). There were also indications that the timing and magnitude of ground evaporation were incorrect (section 4.1), so we conclude that some adjustment to the subcanopy ground evaporation (via modifications to $C_{s,dense}$) are needed.
3. The stability correction to $C_{s,dense}$ suggested by Sakaguchi and Zeng (2009) was found to produce small changes in the CLM fluxes and temperature for the US-NR1 site. Furthermore, this correction

only decreases $C_{s,dense}$, whereas our results suggest that increasing $C_{s,dense}$ would be justified (Figure 13).

4. The measured and modeled friction velocity $u_*$ agreed well during daytime, however, CLM nocturnal $u_*$ was ≈0.3 m $s^{-1}$ whereas observed $u_*$ was ≈0.4 m $s^{-1}$. We circumvented this issue by using observed $u_*$ as an input to CLM, which increased the magnitude of the turbulent fluxes and increased the nocturnal CLM temperatures (thus reducing the issue of a cold canopy temperature bias and runaway cooling).
5. CLM nocturnal latent heat flux in both dry and wet conditions was ≈10 W $m^{-2}$ (i.e., there was not a large increase in $\lambda E$ during wet conditions, as described in (ii) above). Further investigation found that CLM canopy and ground evaporation at night were both very small (Figure 3). Though using observed $u_*$ as input into CLM increased nocturnal $\lambda E$, it did so for both wet and dry conditions. Increasing $C_{s,dense}$ by a factor of 1,000 led to larger nocturnal $\lambda E$ fluxes in wet conditions that approached the observations. Based on a comparison with a forested site in relatively flat terrain (Howland Forest), we hypothesize that the enhanced nocturnal $\lambda E$ at US-NR1 is related to the drainage flow which is not represented within CLM.
6. The comparison with Howland Forest brought to light an important effect of mountainous terrain: slope-generated drainage flows contribute additional turbulent energy which we speculate promotes evaporation and enhances US-NR1 nocturnal latent heat flux.
7. With regard to the universal similarity functions used in CLM4.5: we suggest that rather than limiting $\zeta$ with the variable *zetamaxstable*, it would be more appropriate to use a form of the universal function that is constant in strongly stable conditions (as recommended by Handorf et al. (1999)). For US-NR1, we suggest that the universal function should be constant for $\zeta > 1$.
8. We tested the portion of the CLM4.5 subcanopy parameterization that assumes a linear relationship between velocity on the vegetation $U_{av}$ and above-canopy $u_*$. We found it generally overestimated $U_{av}$ by about a factor of 2 (supporting information Figure S5).
9. In dry conditions, the timing of the diel-cycle peak in CLM $\lambda E$ and soil temperatures were inconsistent with those of the observations (Figure 15). In general, CLM $\lambda E$ followed VPD whereas the peak in observed $\lambda E$ was affected by other phenomena (we suspect entrainment at the top of the boundary layer). Also, the peak in CLM soil temperature was several hours later than the peak in observed $T_{soil}$.
10. From the US-NR1 observations, the cumulative warm-season fluxes suggest that this subalpine forest releases about 300 mm of water and 700 MJ $m^{-2}$ of sensible heat into the atmosphere. Among the 14 CLM configurations considered in our study, the warm-season cumulative water vapor varied by about 8% and sensible heat by 25%.

Our study describes a method of testing land-surface models for appropriate representation of the diel changes in surface energy fluxes when precipitation occurs. This analysis led to further insight into the measurements as well as pin-pointing areas for future model improvement in forested areas. On the measurement side, improved understanding of canopy temperature, better estimates of soil and vegetation evaporation and interception (especially at night), controls on subcanopy turbulent exchange (e.g., Thomas et al., 2013), slope flow dynamics (or more comparisons between flat and sloped sites), as well as better estimates of forest and soil physical properties would be useful. On the modeling side, possible improvements and suggested areas for future work are (1) revisiting the subcanopy turbulent parameterization (e.g., Zeng et al., 2005), (2) taking into account the effect of forest biomass heat capacity on the turbulent fluxes and the surface energy budget (e.g., Leuning et al., 2012), (3) including modifications to the MOST universal functions that take into account the possibility that the uppermost measurement level is within the roughness sublayer (e.g., Harman & Finnigan, 2008), and (4) the inclusion of slope-effects and drainage air flows in complex terrain that lead to increased nocturnal turbulence and surface evaporation. Model development will only progress if data from multiple measurement sites with a wide variety of canopy types and forest densities situated in different landscapes are brought together to create better understanding over a wide parameter space. Observational networks such as FLUXNET (Baldocchi et al., 2001) are well positioned to help in these efforts and much work has already been made in this direction (e.g., Abramowitz et al., 2008; Blyth et al., 2010; Bonan et al., 2011, 2012; Chen & Zhang, 2009; Stöckli et al., 2008; Ukkola et al., 2017; Williams et al., 2009).

## Appendix A: Site-Specific Adjustments to CLM

For the US-NR1 plant type (temperate needleleaf evergreen forest), CLM assumes a canopy height *h* of 17 m. We found that fine-tuning the canopy and observation height (to better match the actual US-NR1 forest) resulted in slightly different results compared to using the default version of CLM4.5. To tune CLM4.5 for use with a specific flux site, the CLM4.5 FORTRAN program "CanopyTemperatureMod.F90" was modified in the following 2 ways:

1. The US-NR1 canopy height of 13 m (*htop* in CLM4.5 source code) was specified and added to the following DO LOOP of CanopyTemperatureMod.F90. This replaces the default value (17 m), which is based on the vegetation type:

```
do  fp = 1,num_nolakep
    p = filter_nolakep(fp)
       !scs: from burns et al 15
       htop(p) = 13.0_r8
       !scs
       z0m(p) = z0mr(patch%itype(p)) * htop(p)
       displa(p) = displar(patch%itype(p)) * htop(p)
end do
```

2. The following lines,

```
         if (frac_veg_nosno(p) == 0) then
            forc_hgt_u_patch(p) = forc_hgt_u(g) + z0mg(c) + displa(p)
            forc_hgt_t_patch(p) = forc_hgt_t(g) + z0mg(c) + displa(p)
            forc_hgt_q_patch(p) = forc_hgt_q(g) + z0mg(c) + displa(p)
         else
            forc_hgt_u_patch(p) = forc_hgt_u(g) + z0m(p) + displa(p)
            forc_hgt_t_patch(p) = forc_hgt_t(g) + z0m(p) + displa(p)
            forc_hgt_q_patch(p) = forc_hgt_q(g) + z0m(p) + displa(p)
         end if
```

are modified so that the forcing height is not adjusted by the displacement and roughness heights. For US-NR1, the observational height is 21.5 m so these lines become:

```
!scs: don't adjust forcing height
         if (frac_veg_nosno(p) == 0) then
            forc_hgt_u_patch(p) = max(forc_hgt_u(g),21.5)
            forc_hgt_t_patch(p) = max(forc_hgt_t(g),21.5)
            forc_hgt_q_patch(p) = max(forc_hgt_q(g),21.5)
         else
            forc_hgt_u_patch(p) = max(forc_hgt_u(g),21.5)
            forc_hgt_t_patch(p) = max(forc_hgt_t(g),21.5)
            forc_hgt_q_patch(p) = max(forc_hgt_q(g),21.5)
         end if
!scs
```

Our modified version of CanopyTemperatureMod.F90 (along with all other modified programs) are included in a ZIP file as described in Appendix C. The modified version of CanopyTemperatureMod.F90 should be placed in the "SourceMods/src.clm/" subdirectory for any particular case where it is to be used.

The effect of varying the canopy height and specifying the observation height of the fluxes and CLM temperatures is shown in Figure A1. Here the CLM4.5 A1 settings are those described in Table 1. CLM4.5 with the "A0" settings uses the default values of a canopy height of 17 m and an observational height that has been adjusted using the momentum roughness and displacement height, as described in (2) above. In

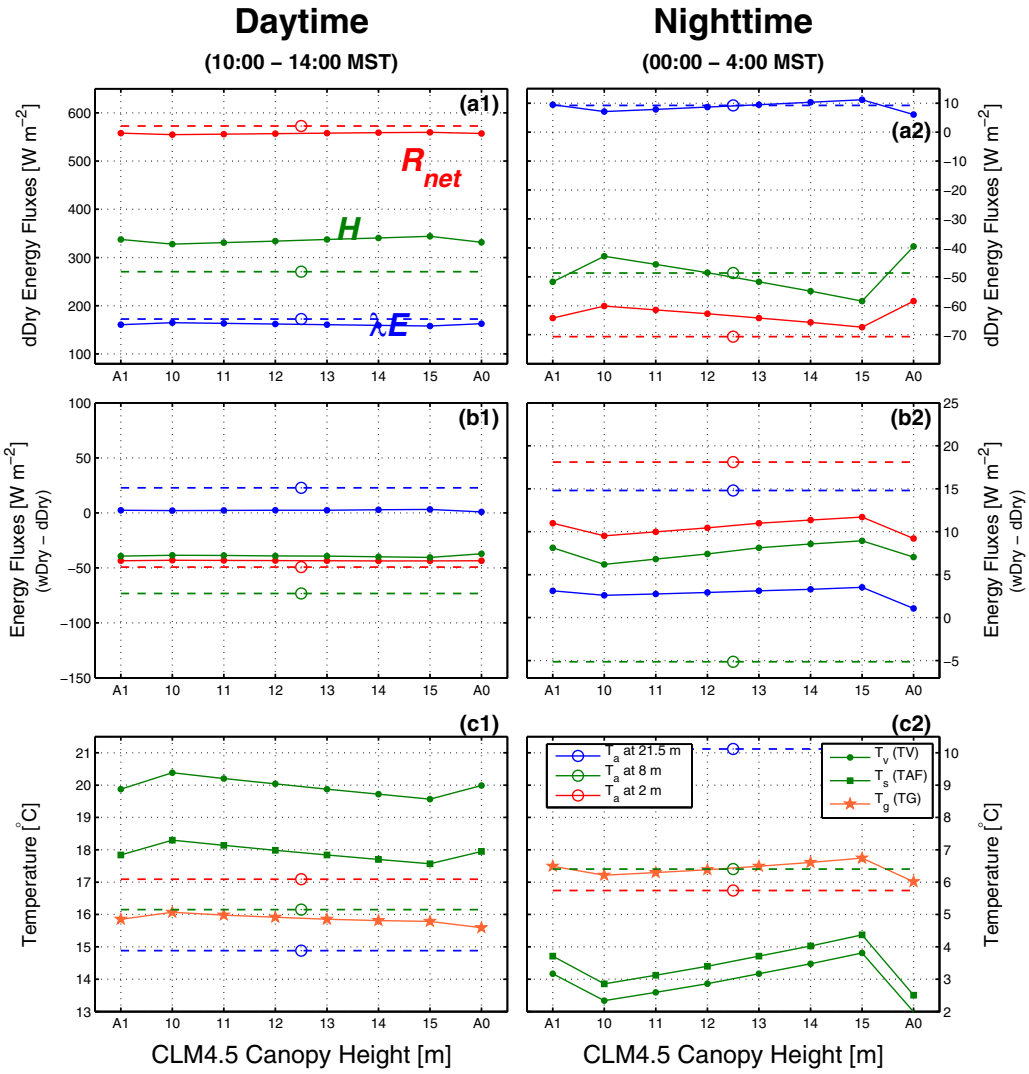


**Figure A1.** (a1, b1) Daytime and (a2, b2) nighttime energy fluxes versus changes to the CLM4.5 canopy height $h$ which has a default value of 17 m. (top) The mean values for dDry conditions and (middle) the mean differences between wDry and dDry conditions where the variables shown are net radiation $R_{net}$ (red), sensible heat flux $H$ (green), and latent heat flux $\lambda E$ (blue). The solid lines with filled symbols are the CLM4.5 output, while the horizontal dashed lines are the US-NR1 observations with an open circle placed at $h = 12.5$ m. (c1, c2) The US-NR1 observed air temperature $T_a$ and the effect of varying $h$ on CLM canopy surface $T_v$, canopy air $T_s$ and ground $T_g$ temperatures are shown (see legends). The A1 column uses the default CLM4.5 settings (see Table 1), whereas the A0 column (on the far-right side) uses the default version of CanopyTemperatureMod.F90, as described in Appendix A.

general, the nocturnal data were more affected than the daytime data by changes to the canopy height, with the changes to nocturnal fluxes on the order of 10–15% (Figure A1a2) and the temperatures changed by around 2°C (Figure A1c2). One of the primary reasons for these changes is that the nocturnal values of friction velocity were increased by around 0.1 m $s^{-1}$ after fine-tuning the CLM forest properties for US-NR1.

## Appendix B: Nomenclature

Table B1 contains the nomenclature, units, and variable descriptions used within our study. It also includes a list all of the variables relevant to our study measured at US-NR1. In some cases, these measured variables are used as input to CLM.

**Table B1**
*A List of Variables in CLM4.5 and Nomenclature Related to Our Study*

| Variable name | CLM4.5 manual equation number | Units | Description and/or equation |
|---|---|---|---|
| *Roman symbols* | | | |
| $C_s$ | 5.115 | Dimensionless | Turbulent transfer coefficient between ground and canopy airspace |
| $C_{s,dense}$ | 5.115 | Dimensionless | Turbulent transfer coefficient between ground and canopy airspace for a dense canopy |
| $d$ | 5.127 | m | Displacement height, prescribed in CLM based on surface type |
| $H$ | Measured, 5.83–5.95 | W m$^{-2}$ | Above-canopy vertical sensible heat flux |
| $L$ | 5.16 | m | Obukhov length, $L=-(u_*^3\,\bar{\theta})/(\kappa g\,\overline{w'\theta'})$ |
| LAI | | m$^2$ m$^{-2}$ | Projected leaf area index, prescribed in CLM based on surface type and satellite data |
| $P$ | Measured | kPa | Barometric pressure (supplied as an input variable to CLM4.5) |
| $R_{\mathrm{net}}$ | Measured, 4.4, 4.17 | W m$^{-2}$ | Above-canopy net irradiance (incoming shortware and longwave irradiance are supplied as input variables to CLM4.5) |
| $RH$ | Measured | % | Above-canopy relative humidity (supplied as an input variable to CLM4.5) |
| $r'_{ah}$ | 5.113 | s m$^{-1}$ | Aerodynamic resistance for heat exchange between ground and canopy |
| $r'_{aw}$ | 5.113 | s m$^{-1}$ | Aerodynamic resistance for water vapor exchange between between ground and canopy ($r'_{ah}=r'_{aw}$) |
| $T_{tc}$ | Measured | °C | Thermocouple temperature (at US-NR1, measured at 11 levels) |
| $T_a$ | Measured | K or °C | Air temperature (measured at US-NR1; the above-canopy air temperature (TBOT) is used as an input variable to CLM4.5) |
| $T_g$ | 6.29–6.32 | K or °C | Ground surface temperature |
| $T_{2m}$ | 5.58 | K or °C | Air temperature at 2 m above the apparent sink for sensible heat ($z_{0h}+d$) |
| $T_s$ | 5.90 | K or °C | Surface temperature (at height ($z_{0h}+d$)), or canopy air temperature |
| $T_{soil}$ | Measured, 6.12 | K or °C | Soil temperature (measured at −5 cm at US-NR1; in CLM4.5, calculated at 15 depths below the surface) |
| $T_v$ | | K or °C | Vegetation temperature |
| $q$ | Measured | g kg$^{-1}$ | Atmospheric specific humidity (at US-NR1, measured at 21.5 m) |
| $q_*$ | 5.15 | g kg$^{-1}$ | Humidity scale |
| $u_*$ | Measured, 5.32–5.35 | m s$^{-1}$ | Above-canopy friction velocity, $u_*=((\overline{u'w'})^2+(\overline{v'w'})^2)^{0.25}$ |
| $U_{av}$ | 5.114 | m s$^{-1}$ | Velocity of air within foliage ($U_{av}=u_*$) |
| $U$ | Measured | m s$^{-1}$ | Horizontal wind velocity (at US-NR1, measured at 3 heights (21.5, 5.7, and 2.5 m); above-canopy (21.5 m) $U$ is an input variable to CLM4.5) |
| $u$, $v$, $w$ | Measured | m s$^{-1}$ | Streamwise, crosswise, and vertical planar-fit wind components (at US-NR1, measured at 3 heights: 21.5, 5.7, and 2.5 m) |
| VPD | Measured | kPa | Vapor pressure deficit |
| $z$ | | m | Height above the ground |
| $z_{0m}$ | 5.126 | m | Roughness length for momentum |
| *Greek symbols* | | | |
| $\kappa$ | | Dimensionless | von Kármán constant; in CLM4.5 $\kappa=0.4$ |
| $\lambda$ | Table 2.6 | kJ kg$^{-1}$ | Latent heat of vaporization of water vapor; for US-NR1, $\lambda$ was calculated with $\lambda = 1,000,000\,(2.501-0.00237\,T_a)$ which is for liquid water, with $T_a$ in °C |
| $\lambda E$ | Measured, 5.96, 5.97 | W m$^{-2}$ | Above-canopy vertical latent heat flux ($\lambda E=\lambda E_v^t+\lambda E_v^w+\lambda E_g$) |
| $\lambda E_v^t$ | 5.135 | W m$^{-2}$ | Canopy transpiration |
| $\lambda E_v^w$ | 5.111 | W m$^{-2}$ | Canopy evaporation |
| $\lambda E_g$ | 5.112 | W m$^{-2}$ | Ground evaporation |
| $\phi_m$, $\phi_h$, $\phi_w$ | 5.30–5.31 | Dimensionless | Universal functions for momentum, heat, and moisture (see Table 3) |
| $\psi_m$, $\psi_h$, $\psi_w$ | 5.36–5.45 | Dimensionless | Integral of the universal function for momentum, heat, and moisture (see Table 3) |
| $\theta$ | | K or °C | Potential temperature |
| $\theta_*$ | 5.14 | K or °C | Temperature scale |
| $\zeta$ | Measured, 5.48–5.49 | Dimensionless | Above-canopy stability parameter ($\zeta=(z-d)/L$) |

*Note*. Where appropriate, equation numbers from the CLM4.5 manual (Oleson et al., 2013) are listed. If the variable is measured at the US-NR1 site, then "Measured" is included within this same column. Mean values are shown with an overbar ($\bar{x}$) and turbulent fluctuations from a mean are indicated by a prime ($x'$); if neither are shown a total or mean value should be assumed.

## Appendix C: Data and Software Sources

The observational data used in our study are available from AmeriFlux (http://ameriflux.lbl.gov/) where the two sites we have used are US-NR1 (https://doi.org/10.17190/AMF/1246088) and US-Ho1 (https://doi.org/10.17190/AMF/1246061). Different versions of the CLM model can be found at http://www.cesm.ucar.edu/models/clm/. Within the supporting information, we have included more information about our modifications to the CLM4.5 source code, as well as the modified code in a zip file, agu_JAMES_SpB_CLM_code_mods_180110.zip.

**Acknowledgments**
We thank Thomas Foken and Arnold Moene for useful discussions related to our study. We also thank Dave Hollinger and his team at Howland Forest for the US-Ho1 data. Appendix C contains information about how to obtain the data and CLM model used in our study. The comments from two anonymous reviewers improved this paper. The US-NR1 AmeriFlux site (and this study) has been supported by the U.S. DOE, Office of Science through the AmeriFlux Management Project (AMP) at Lawrence Berkeley National Laboratory under award 7094866. For this work, S.B. has also been partially supported by NIFA/USDA grant 2015–67003-23485 and the NCAR Mesoscale and Microscale Meteorology (MMM) Laboratory through the Directors reserve account. W.W. was supported by NSF grant DEB 1637686 to the Niwot Ridge LTER. Publication of this article was partially funded by the University of Colorado Boulder Libraries Open Access Fund. The National Center for Atmospheric Research (NCAR) is sponsored by NSF.

## References

Abramowitz, G., Leuning, R., Clark, M., & Pitman, A. (2008). Evaluating the performance of land surface models. *Journal of Climate*, *21*, 5468–5481.

Aubinet, M. (2008). Eddy covariance $CO_2$ flux measurements in nocturnal conditions: An analysis of the problem. *Ecological Applications*, *18*, 1368–1378.

Aubrecht, D. M., Helliker, B. R., Goulden, M. L., Roberts, D. A., Still, C. J., & Richardson, A. D. (2016). Continuous, long-term, high-frequency thermal imaging of vegetation: Uncertainties and recommended best practices. *Agricultural and Forest Meteorology*, *228–229*, 315–326. https://doi.org/10.1016/j.agrformet.2016.07.017

Baas, P., Steeneveld, G. J., van de Wiel, B. J. H., & Holtslag, A. A. M. (2006). Exploring self-correlation in flux-gradient relationships for stably stratified conditions. *Journal of the Atmospheric Sciences*, *63*, 3045–3054. https://doi.org/10.1175/JAS3778.1

Baldocchi, D., Falge, E., Gu, L. H., Olson, R., Hollinger, D., Running, S., et al. (2001). FLUXNET: A new tool to study the temporal and spatial variability of ecosystem-scale carbon dioxide, water vapor, and energy flux densities. *Bulletin of the American Meteorological Society*, *82*, 2415–2434.

Betts, A. K. (2009). Land-surface-atmosphere coupling in observations and models. *Journal of Advances in Modeling Earth Systems*, *1*, 4. https://doi.org/10.3894/JAMES.2009.1.4

Betts, A. K., & Ball, J. H. (1995). The FIFE surface diurnal cycle climate. *Journal of Geophysical Research*, *100*, 25679–25693.

Blanken, P. D., Monson, R. K., Burns, S. P., & Turnipseed, A. A. (1998-present). *Data and information for the AmeriFlux US-NR1 Niwot Ridge Subalpine Forest (LTER NWT1) site, AmeriFlux Management Project*. Berkeley, CA: Lawrence Berkeley National Laboratory. https://doi.org/10.17190/AMF/1246088

Blanken, P. D., Rouse, W. R., & Schertzer, W. M. (2003). Enhancement of evaporation from a large northern lake by the entrainment of warm, dry air. *Journal of Hydrometeorology*, *4*, 680–693.

Blyth, E., Gash, J., Lloyd, A., Pryor, M., Weedon, G. P., & Shuttleworth, J. (2010). Evaluating the JULES land surface model energy fluxes using FLUXNET data. *Journal of Hydrometeorology*, *11*, 509–519.

Bonan, G. B. (1996). *A Land Surface Model (LSM version 1.0) for ecological, hydrological, and atmospheric studies: Technical description and user's guide* (Tech. Rep. NCAR/TN-417+STR, 150 pp.). Boulder, CO: National Center for Atmospheric Research. https://doi.org/10.5065/D6DF6P5X

Bonan, G. B. (2008). *Ecological climatology: Concepts and applications* (2nd ed., 550 pp.). Cambridge, UK: Cambridge University Press.

Bonan, G. B., Lawrence, P. J., Oleson, K. W., Levis, S., Jung, M., Reichstein, M., et al. (2011). Improving canopy processes in the Community Land Model version 4 (CLM4) using global flux fields empirically inferred from FLUXNET data. *Journal of Geophysical Research: Biogeosciences*, *116*, G02014. https://doi.org/10.1029/2010JG001593

Bonan, G. B., Oleson, K. W., Fisher, R. A., Lasslop, G., & Reichstein, M. (2012). Reconciling leaf physiological traits and canopy flux data: Use of the TRY and FLUXNET databases in the Community Land Model version 4. *Journal of Geophysical Research: Biogeosciences*, *117*, G02026. https://doi.org/10.1029/2011JG001913

Bonan, G. B., Patton, E. G., Harman, I. N., Oleson, K. W., Finnigan, J. J., Lu, Y., & Burakowski, E. A. (2017). Modeling canopy-induced turbulence in the Earth system: A unified parameterization of turbulent exchange within plant canopies and the roughness sublayer (CLM-ml v0). *Geoscientific Model Development Discussion*, *2017*, 1–80. https://doi.org/10.5194/gmd-2017-261

Bonan, G. B., Williams, M., Fisher, R. A., & Oleson, K. W. (2014). Modeling stomatal conductance in the earth system: Linking leaf water-use efficiency and water transport along the soil-plant-atmosphere continuum. *Geoscientific Model Development*, *7*, 2193–2222.

Bosveld, F. C., & Bouten, W. (2003). Evaluating a model of evaporation and transpiration with observations in a partially wet Douglas-fir forest. *Boundary-Layer Meteorology*, *108*, 365–396.

Bowling, D. R., Logan, B. A., Hufkens, K., Aubrecht, D. M., Richardson, A. D., Burns, S. P., et al. (2018). Limitations to winter and spring photosynthesis of a Rocky Mountain subalpine forest. *Agricultural and Forest Meteorology*, *252*, 241–255. https://doi.org/10.1016/j.agrformet.2018.01.025

Brutsaert, W. (1982). *Evaporation into the atmosphere* (299 pp.). Dordrecht, the Netherlands: Kluwer Academic.

Burns, S. P., Blanken, P. D., Turnipseed, A. A., Hu, J., & Monson, R. K. (2015). The influence of warm-season precipitation on the diel cycle of the surface energy balance and carbon dioxide at a Colorado subalpine forest site. *Biogeosciences*, *12*, 7349–7377. https://doi.org/10.5194/bg-12-7349-2015

Burns, S. P., Sun, J., Lenschow, D. H., Oncley, S. P., Stephens, B. B., Yi, C., et al. (2011). Atmospheric stability effects on wind fields and scalar mixing within and just above a subalpine forest in sloping terrain. *Boundary-Layer Meteorology*, *138*, 231–262. https://doi.org/10.1007/s10546-010-9560-6

Businger, J. A., Wyngaard, J. C., Izumi, Y., & Bradley, E. F. (1971). Flux-profile relationships in atmospheric surface layer. *Journal of the Atmospheric Sciences*, *28*, 181–189.

Chen, F., & Zhang, Y. (2009). On the coupling strength between the land surface and the atmosphere: From viewpoint of surface exchange coefficients. *Geophysical Research Letters*, *36*, L10404.

Clark, M. P., Fan, Y., Lawrence, D. M., Adam, J. C., Bolster, D., Gochis, D. J., et al. (2015). Improving the representation of hydrologic processes in Earth System Models. *Water Resources Research*, *51*, 5929–5956. https://doi.org/10.1002/2015WR017096

Dickinson, R. E., Henderson-Sellers, A., & Kennedy, P. J. (1993). *Biosphere-Atmosphere Transfer Scheme (BATS) version 1e as coupled to the NCAR Community Climate Model* (Tech. Rep. NCAR/TN-387+STR, 72 pp.). Boulder, CO: National Center for Atmospheric Research. https://doi.org/10.5065/D67W6959

Finnigan, J. (2008). An introduction to flux measurements in difficult conditions. *Ecological Applications*, *18*, 1340–1350.

Foken, T. (2006). 50 years of the Monin-Obukhov Similarity Theory. *Boundary-Layer Meteorology*, *119*, 431–447.

Foken, T. (2008). *Micrometeorology* (308 pp.). Heidelberg, Germany: Springer.
Froelich, N. J., & Schmid, H. P. (2006). Flow divergence and density flows above and below a deciduous forest. Part II. Below-canopy thermotopographic flows. *Agricultural and Forest Meteorology*, *138*, 29–43.
Gable, D. J., & Madole, R. F. (1976). *Geologic map of the Ward quadrangle* (Geologic Quadrangle Map GQ-1277; scale 1:24,000, digital media). Boulder, CO: U.S. Geological Survey.
Gentine, P., Entekhabi, D., & Polcher, J. (2011). The diurnal behavior of evaporative fraction in the soil-vegetation-atmospheric boundary layer continuum. *Journal of Hydrometeorology*, *12*, 1530–1546. https://doi.org/10.1175/2011JHM1261.1
Grelle, A., Lundberg, A., Lindroth, A., Moren, A. S., & Cienciala, E. (1997). Evaporation components of a boreal forest: Variations during the growing season. *Journal of Hydrology*, *197*, 70–87.
Handorf, D., Foken, T., & Kottmeier, C. (1999). The stable atmospheric boundary layer over an Antarctic ice sheet. *Boundary-Layer Meteorology*, *91*, 165–189.
Harman, I. N., & Finnigan, J. J. (2007). A simple unified theory for flow in the canopy and roughness sublayer. *Boundary-Layer Meteorology*, *123*, 339–363.
Harman, I. N., & Finnigan, J. J. (2008). Scalar concentration profiles in the canopy and roughness sublayer. *Boundary-Layer Meteorology*, *129*, 323–351.
Högström, U. (1988). Non-dimensional wind and temperature profiles in the atmospheric surface layer: A re-evaluation. *Boundary-Layer Meteorology*, *42*, 55–78.
Hollinger, D. (1996-present). *Data and information for the AmeriFlux US-Ho1 Howland Forest (main tower) site, AmeriFlux Management Project*. Berkeley, CA: Lawrence Berkeley National Laboratory. https://doi.org/10.17190/AMF/1246061
Hollinger, D. Y., Aber, J., Dail, B., Davidson, E. A., Goltz, S. M., Hughes, H., et al. (2004). Spatial and temporal variability in forest-atmosphere $CO_2$ exchange. *Global Change Biology*, *10*, 1689–1706.
Hollinger, D. Y., Goltz, S. M., Davidson, E. A., Lee, J. T., Tu, K., & Valentine, H. T. (1999). Seasonal patterns and environmental control of carbon dioxide and water vapour exchange in an ecotonal boreal forest. *Global Change Biology*, *5*, 891–902.
Holtslag, A. A. M., Svensson, G., Baas, P., Basu, S., Beare, B., Beljaars, A. C. M., et al. (2013). Stable atmospheric boundary layers and diurnal cycles challenges for weather and climate models. *Bulletin of the American Meteorological Society*, *94*, 1691–1706.
Kaimal, J. C., & Finnigan, J. J. (1994). *Atmospheric boundary layer flows: Their structure and measurement* (289 pp.). New York, NY: Oxford University Press.
Kang, M., Kwon, H., Cheon, J. H., & Kim, J. (2012). On estimating wet canopy evaporation from deciduous and coniferous forests in the Asian monsoon climate. *Journal of Hydrometeorology*, *13*, 950–965.
Kim, Y., Still, C. J., Hanson, C. V., Kwon, H., Greer, B. T., & Law, B. E. (2016). Canopy skin temperature variations in relation to climate, soil temperature, and carbon flux at a ponderosa pine forest in central Oregon. *Agricultural and Forest Meteorology*, *226*, 161–173.
Klaassen, W. (2001). Evaporation from rain-wetted forest in relation to canopy wetness, canopy cover, and net radiation. *Water Resources Research*, *37*, 3227–3236.
Knowles, J. F., Burns, S. P., Blanken, P. D., & Monson, R. K. (2015a). Fluxes of energy, water, and carbon dioxide from mountain ecosystems at Niwot Ridge, Colorado. *Plant Ecology & Diversity*, *8*, 663–676. https://doi.org/10.1080/17550874.2014.904950
Knowles, J. F., Harpold, A. A., Cowie, R., Zeliff, M., Barnard, H. R., Burns, S. P., et al. (2015b). The relative contributions of alpine and subalpine ecosystems to the water balance of a mountainous, headwater catchment. *Hydrological Processes*, *29*, 4794–4808. https://doi.org/10.1002/hyp.10526
Kume, T., Manfroi, O. J., Suzuki, M., Tanaka, K., Kuraji, K., Nakagawa, M., et al. (2008). Estimation of vertical profiles of leaf drying times after daytime rainfall within a Bornean tropical rainforest. *Hydrological Processes*, *22*, 3689–3696. https://doi.org/10.1002/hyp.6972
Lawrence, D. M., Oleson, K. W., Flanner, M. G., Thornton, P. E., Swenson, S. C., Lawrence, P. J., et al. (2011). Parameterization improvements and functional and structural advances in version 4 of the Community Land Model. *Journal of Advances in Modeling Earth Systems*, *3*, M03001. https://doi.org/10.1029/2011MS00045
Lawrence, D. M., Thornton, P. E., Oleson, K. W., & Bonan, G. B. (2007). The partitioning of evapotranspiration into transpiration, soil evaporation, and canopy evaporation in a GCM: Impacts on land-atmosphere interaction. *Journal of Hydrometeorology*, *8*, 862–880.
Leuning, R., van Gorsel, E., Massman, W. J., & Isaac, P. R. (2012). Reflections on the surface energy imbalance problem. *Agricultural and Forest Meteorology*, *156*, 65–74. https://doi.org/10.1016/j.agrformet.2011.12.002
Lindroth, A., Molder, M., & Lagergren, F. (2010). Heat storage in forest biomass improves energy balance closure. *Biogeosciences*, *7*, 301–313.
Lo Seen, D., Chehbouni, A., Njoku, E., Saatchi, S., Mougin, E., & Monteny, G. (1997). An approach to couple vegetation functioning and soil-vegetation-atmosphere-transfer models for semiarid grasslands during the HAPEX-Sahel experiment. *Agricultural and Forest Meteorology*, *83*, 49–74.
Madole, R. F. (1969). Pinedale and Bull Lake glaciation in Upper St. Vrain drainage basin, Boulder County, Colorado. *Arctic Antarctic and Alpine Research*, *4*, 279–287.
Mahrt, L. (1999). Stratified atmospheric boundary layers. *Boundary-Layer Meteorology*, *90*, 375–396.
Marr, J. W. (1961). *Ecosystems on the east slope of the Front Range in Colorado, Series in Biology* (No. 8, 144 pp.). Boulder: University of Colorado Press.
Matheny, A. M., Bohrer, G., Stoy, P. C., Baker, I. T., Black, A. T., Desai, A. R., et al. (2014). Characterizing the diurnal patterns of errors in the prediction of evapotranspiration by several land-surface models: An NACP analysis. *Journal of Geophysical Research: Biogeosciences*, *119*, 1458–1473. https://doi.org/10.1002/2014JG002623
Moene, A. F., & Van Dam, J. C. (2014). *Transport in the atmosphere-vegetation-soil continuum* (458 pp.). New York, NY: Cambridge University Press.
Monson, R. K., Prater, M. R., Hu, J., Burns, S. P., Sparks, J. P., Sparks, K. L., et al. (2010). Tree species effects on ecosystem water-use efficiency in a high-elevation, subalpine forest. *Oecologia, 162*, 491–504. https://doi.org/10.1007/s00442-009-1465-z
Monson, R. K., Turnipseed, A. A., Sparks, J. P., Harley, P. C., Scott-Denton, L. E., Sparks, K., et al. (2002). Carbon sequestration in a high-elevation, subalpine forest. *Global Change Biology*, *8*, 459–478.
Moors, E. J. (2012). *Water use of forests in the Netherlands* (PhD thesis, 290 pp.). Amsterdam, the Netherlands: Vrije Universiteit.
Novick, K. A., Oren, R., Stoy, P. C., Siqueira, M. B. S., & Katul, G. G. (2009). Nocturnal evapotranspiration in eddy-covariance records from three co-located ecosystems in the Southeastern U.S.: Implications for annual fluxes. *Agricultural and Forest Meteorology*, *149*, 1491–1504.
Oleson, K. W., Lawrence, D. M., Bonan, G. B., Drewniak, B., Huang, M., Koven, C. D., et al. (2013). *Technical description of version 4.5 of the Community Land Model (CLM)* (Tech. Rep. NCAR/TN-503+STR, 420 pp.). Boulder, CO: National Center for Atmospheric Research. https://doi.org/10.5065/D6RR1W7M

Oleson, K. W., Niu, G. Y., Yang, Z. L., Lawrence, D. M., Thornton, P. E., Lawrence, P. J., et al. (2008). Improvements to the Community Land Model and their impact on the hydrological cycle. *Journal of Geophysical Research: Biogeosciences*, *113*, G01021. https://doi.org/10.1029/2007JG000563

Panofsky, H. A., & Dutton, J. A. (1984). *Atmospheric turbulence: Models and methods for engineering applications* (397 pp.). New York, NY: Wiley Interscience.

Patton, E. G., Sullivan, P. P., Shaw, R. H., Finnigan, J. J., & Weil, J. C. (2016). Atmospheric stability influences on coupled boundary layer and canopy turbulence. *Journal of the Atmospheric Sciences*, *73*, 1621–1647.

Pyles, R. D., Weare, B. C., & Paw U, K. T. (2000). The UCD Advanced Canopy-Atmosphere-Soil Algorithm: Comparisons with observations from different climate and vegetation regimes. *Quarterly Journal of the Royal Meteorological Society*, *126*, 2951–2980.

Raczka, B., Duarte, H. F., Koven, C. D., Ricciuto, D., Thornton, P. E., Lin, J. C., et al. (2016). An observational constraint on stomatal function in forests: Evaluating coupled carbon and water vapor exchange with carbon isotopes in the Community Land Model (CLM4.5). *Biogeosciences*, *13*(18), 5183–5204. https://doi.org/10.5194/bg-13-5183-2016

Raupach, M. R., & Finnigan, J. J. (1988). Single-layer models of evaporation from plant canopies are incorrect but useful, whereas multilayer models are correct but useless: Discuss. *Australian Journal of Plant Physiology*, *15*, 705–716.

Raupach, M. R., Finnigan, J. J., & Brunet, Y. (1996). Coherent eddies and turbulence in vegetation canopies: The mixing-layer analogy. *Boundary-Layer Meteorology*, *78*, 351–382.

Rutter, A. J., Morton, A. J., & Robins, P. C. (1975). A predictive model of rainfall interception in forests. II. Generalization of model and comparison with observations in some coniferous and hardwood stands. *Journal of Applied Ecology*, *12*, 367–380.

Sakaguchi, K., & Zeng, X. (2009). Effects of soil wetness, plant litter, and under-canopy atmospheric stability on ground evaporation in the Community Land Model (CLM3.5). *Journal of Geophysical Research: Atmospheres*, *114*, D01107. https://doi.org/10.1029/2008JD010834

Scott-Denton, L. E., Sparks, K. L., & Monson, R. K. (2003). Spatial and temporal controls of soil respiration rate in a high-elevation, subalpine forest. *Soil Biology & Biochemistry*, *35*, 525–534.

Shaw, R. H., & Zhang, X. J. (1992). Evidence of pressure-forced turbulent-flow in a forest. *Boundary-Layer Meteorology*, *58*, 273–288.

Shuttleworth, W. J. (2007). Putting the 'vap' into evaporation. *Hydrology and Earth System Sciences*, *11*, 210–244.

Stewart, J. B. (1977). Evaporation from wet canopy of a pine forest. *Water Resources Research*, *13*, 915–921.

Stöckli, R., Lawrence, D. M., Niu, G. Y., Oleson, K. W., Thornton, P. E., Yang, Z. L., et al. (2008). Use of FLUXNET in the Community Land Model development. *Journal of Geophysical Research: Biogeosciences*, *113*, G01025. https://doi.org/10.1029/2007JG000562

Sun, J., Burns, S. P., Delany, A. C., Oncley, S. P., Turnipseed, A. A., Stephens, B. B., et al. (2007). $CO_2$ transport over complex terrain. *Agricultural and Forest Meteorology*, *145*, 1–21. https://doi.org/10.1016/j.agrformet.2007.02.007

Swenson, S. C., & Lawrence, D. M. (2014). Assessing a dry surface layer-based soil resistance parameterization for the Community Land Model using GRACE and FLUXNET-MTE data. *Journal of Geophysical Research: Atmospheres*, *119*, 10299–10312. https://doi.org/10.1002/2014JD022314

Thomas, C. K., Martin, J. G., Law, B. E., & Davis, K. (2013). Toward biologically meaningful net carbon exchange estimates for tall, dense canopies: Multi-level eddy covariance observations and canopy coupling regimes in a mature Douglas-fir forest in Oregon. *Agricultural and Forest Meteorology*, *173*, 14–27. https://doi.org/10.1016/j.agrformet.2013.01.001

Tolk, J. A., Howell, T. A., & Evett, S. R. (2006). Nighttime evapotranspiration from alfalfa and cotton in a semiarid climate. *Agronomy Journal*, *98*, 730–736.

Turnipseed, A. A., Anderson, D. E., Blanken, P. D., Baugh, W. M., & Monson, R. K. (2003). Airflows and turbulent flux measurements in mountainous terrain. Part 1. Canopy and local effects. *Agricultural and Forest Meteorology*, *119*, 1–21.

Turnipseed, A. A., Blanken, P. D., Anderson, D. E., & Monson, R. K. (2002). Energy budget above a high-elevation subalpine forest in complex topography. *Agricultural and Forest Meteorology*, *110*, 177–201.

Turnipseed, A. A., Burns, S. P., Moore, D. J. P., Hu, J., Guenther, A. B., & Monson, R. K. (2009). Controls over ozone deposition to a high elevation subalpine forest. *Agricultural and Forest Meteorology*, *149*, 1447–1459. https://doi.org/10.1016/j.agrformet.2009.04.001

Ukkola, A. M., Haughton, N., De Kauwe, M. G., Abramowitz, G., & Pitman, A. J. (2017). FluxnetLSM R package (v1.0): A community tool for processing FLUXNET data for use in land surface modelling. *Geoscientific Model Development*, *10*, 3379–3390. https://doi.org/10.5194/gmd-10-3379-2017

van Dijk, A. I. J. M., Gash, J. H., van Gorsel, E., Blanken, P. D., Cescatti, A., Emmel, C., et al. (2015). Rainfall interception and the coupled surface water and energy balance. *Agricultural and Forest Meteorology*, *214*, 402–415.

van Heerwaarden, C. C., Vilà-Guerau de Arellano, J., Gounou, A., Guichard, F., & Couvreux, F. (2010). Understanding the daily cycle of evapotranspiration: A new method to quantify the influence of forcings and feedbacks. *Journal of Hydrometeorology*, *11*, 1405–1422. https://doi.org/10.1175/2010JHM1272.1

Williams, M., Richardson, A. D., Reichstein, M., Stoy, P. C., Peylin, P., Verbeeck, H., et al. (2009). Improving land surface models with FLUXNET data. *Biogeosciences*, *6*, 1341–1359.

Yi, C., Anderson, D. E., Turnipseed, A. A., Burns, S. P., Sparks, J. P., Stannard, D. I., et al. (2008). The contribution of advective fluxes to net ecosystem exchange in a high-elevation, subalpine forest. *Ecological Applications*, *18*, 1379–1390. https://doi.org/10.1890/06-0908.1

Yi, C., Monson, R. K., Zhai, Z. Q., Anderson, D. E., Lamb, B., Allwine, G., et al. (2005). Modeling and measuring the nocturnal drainage flow in a high-elevation, subalpine forest with complex terrain. *Journal of Geophysical Research: Atmospheres*, *110*, D22303. https://doi.org/10.1029/2005JD006282

Zeng, X., Dickinson, R. E., Barlage, M., Dai, Y. J., Wang, G. L., & Oleson, K. (2005). Treatment of undercanopy turbulence in land models. *Journal of Climate*, *18*, 5086–5094.

Zeng, X., Zhao, M., & Dickinson, R. E. (1998). Intercomparison of bulk aerodynamic algorithms for the computation of sea surface fluxes using TOGA COARE and TAO data. *Journal of Climate*, *11*, 2628–2644. https://doi.org/10.1175/1520-0442(1998)011<2628:IOBAAF>2.0.CO;2